



รายงานวิจัยฉบับสมบูรณ์

โครงการ: การออกแบบและการหาค่าที่เหมาะสมขั้นต้นของเครื่องบินรบไร้คนขับชนิดปึกบิน Conceptual Design Synthesis and Optimization of Flying Wing Unmanned Combat Air Vehicle

โดย ผศ.ศร. บุญชัย วัจจะตรากุล และคณะ

รายงานวิจัยฉบับสมบูรณ์

โครงการ: การออกแบบและการหาค่าที่เหมาะสมขั้นต้นของเครื่องบินรบไร้คนขับชนิดปึกบิน Conceptual Design Synthesis and Optimization of Flying Wing Unmanned Combat Air Vehicle

คณะผู้วิจัย

- ผศ.ดร. บุญชัย วัจจะดรากุล
 (หัวหน้าโครงการวิจัยผู้รับทุน)
- ผศ.ดร. อุดมเกียรดิ นนทแกัว (นักวิจัยที่ปรึกษา)
- Dr. Howard Smith

 (นักวิจัยที่ปรึกษา)

สังกัด

ภาควิชาวิศวกรรมเครื่องกล สถาบันเทคโนโลยีพระจอมเกล้าพระนครเหนือ

ภาควิชาวิศวกรรมเครื่องกล สถาบันเทคโนโลยีพระจอมเกล้าพระนครเหนือ

School of Engineering, Cranfield University, England

สนับสนุนโดยสำนักงานคณะกรรมการการอุดมศึกษา และ สำนักงานกองทุนสนับสนุนการวิจัย (ความเห็นในรายงานนี้เป็นของผู้วิจัย สกอ และ สกว. ไม่จำเป็นต้องเห็นด้วยเสมอไป)

บทคัดย่อ

ในปัจจุบันเป็นที่ขอมรับกันโดยทั่วไปว่า เครื่องบินรบไร้คนขับ (Unmanned Combat Air Vehicle, UCAV)

มีข้อได้เปรียบเหนือกว่าเครื่องบินรบทั่วไปที่ใช้ในปัจจุบันและมีแนวโน้มว่าเครื่องบินรบไร้คนขับนั้นจะถูกนำมาใช้
ในการทำการรบในอนาคตอันใกล้นี้ การที่ไม่มีนักบินบนเครื่องบินทำให้เครื่องบินรบไร้คนขับมีความเหมาะสมกับ
การกิจที่เกี่ยงอันตราย ซึ่งอาจจะทำให้นักบินถูกจับหรือเสียชีวิตได้และการที่ไม่มีนักบินบนเครื่องบินนั้นทำให้
เครื่องบินสามารถที่จะถูกออกแบบให้มีประสิทธิภาพมากขึ้น มีขนาดเล็กลง น้ำหนักลดลง และราดาถูกลง
นอกจากนี้เครื่องบินรบไร้คนขับนั้นยังสามารถนำกลับมาใช้ในการรบได้หลายครั้งซึ่งเป็นข้อได้ เปรียบเหนือการใช้
จรวจขีปนาวุธในการรบอีกด้วย เครื่องบินที่มีรูปร่างลักษณะเป็นแบบปิกบินได้รับความสนใจที่จะนำมาใช้เป็น
เครื่องบินรบไร้คนขับเป็นอย่างมากเนื่องจากประสิทธิภาพด้านอากาศพลศาสตร์ที่ดีกว่า และการมีคุณลักษณะในการ
อำพรางตัวโดยธรรมชาติของรูปร่างปิกบิน ดังนั้นในการวิจัยในครั้งนี้จึงได้มุ่งเน้นไปถึงการศึกษาการออกแบบ
ขั้นด้นของเครื่องบินรบไร้คนขับชนิดปิกบิน

ในการศึกษาในครั้งนี้โปรแกรมการออกแบบและหาค่าที่เหมาะสมขั้นต้นของเครื่องบินรบไร้คนขับชนิด ปีกบินได้ถูกพัฒนาขึ้นเพื่อศึกษาถึงอิทธิพลของข้อกำหนดและความค้องการในการออกแบบ และศึกษาคุณลักษณะ เฉพาะของเครื่องบีนประเภทปีกบิน โปรแกรมนี้สามารถที่จะจำลองปีกบินที่เป็นแบบ cranked wing โดยใช้ โครงสร้างภายในของปีกอย่างง่ายซึ่งประกอบค้วยคามหน้า คามหลัง และโครงขวาง และมีช่องบรรจุขีปนาวุช ภายในอยู่ด้านล่างของห้องเครื่องยนต์ที่ถึงกลางลำตัวของเครื่องบิน วิธีการคำนวณหาน้ำหนักโครงสร้างของปีกแบบ cranked wing ได้ถูกพัฒนาขึ้นและนำมาใช้ทำให้การประมาณค่าน้ำหนักโครงสร้างของปีกมีความแม่นยำมากยิ่งขึ้น ภาระด้านอากาศพลศาสตร์ถูกด้านวณจากทฤษฎีพื้นผิวแรงชก (lifting-surface theory) ที่สอดคล้องกับรูปร่างของปีก เสถียรภาพและการควบคุมการบินในแกนยาว แกนขวางและแถนคิ่งได้ถูกนำมาพิจารณาในการ ออกแบบ โดยการใช้ elevons ทั้งในการควบกุมการขึ้น-ลงของหัวเครื่อง (pitch control) และการเลี้ยว (roll control) และใช้ split-drag sudders ในการควบคุมทิศทางของหัวเครื่อง (directional control) ขบวมการในการหาคำที่ เหมาะสมจะใช้โปรแกรม LSGRG optimizer เชื่อมต่อกับส่วนในการออกแบบ (design synthesis) โดยใช้น้ำหนัก ของเครื่องบินก่อนวิ่งขึ้น (takeoff mass) เป็นตัวบ่งชี้ถึงเครื่องบินที่เหมาะสมที่สุด (optimum design) ซึ่งเครื่องบิน จะต้องมีน้ำหนักของเครื่องก่อนวิ่งขึ้นน้อยที่สุดภายใต้เงื่อนไขในการออกแบบที่กำหนดไว้ โปรแกรมที่พัฒนาขึ้นนี้พบว่า การขอมให้เสถียรภาพในแนวแกนยาวลคลง จะส่งผลให้เครื่องบินมีขนาคเล็กลงและ น้ำหนักลดลงซึ่งทำให้ประสิทธิภาพของเครื่องบินดีขึ้น นอกจากนี้ยังพบว่ามุมสู่ปักของเครื่องบินชนิดปักบินนั้นถูก กำหนคโดยความต้องการด้านเสถียรภาพมากกว่าความต้องการที่จะลดแรงต้านอากาศพลศาสตร์เช่นปรากฏในเครื่อง บินประเภทอื่น จาการศึกษาในครั้งนี้ยังพบว่าปีกที่มี single leading-edge cranked planform ซึ่งมีมุมภูปิกค้านในและ ด้านนอกที่ไม่เท่ากันนั้น มีความเหมาะสมกับเครื่องบินที่ต้องการบินระยะทางไกลหรือต้องการบรรทุกน้ำหนักมากๆ ทั้งนี้เนื่องจากการที่มุมสูปีกของปีกด้านนอกสามารถออกแบบให้มีขนาดน้อย ซึ่งทำให้มีประสิทธิภาพด้านอากาศ พลศาสตร์ที่ดีขึ้น และยังทำให้มีความยืดหยุ่นในการควบคุมตำแหน่งของจุดศูนย์กลางน้ำหนักและเสถียรภาพในการ บินที่มากขึ้น โปรแกรมที่พัฒนาขึ้นนี้สามารถนำไปใช้ในการศึกษาผลกระทบของการเปลี่ยนแปลงค่าตัวแปรในการ ออกแบบ ความค้องการและเงื่อนไขข้อจำกัดในการออกแบบต่อเครื่องบินซึ่งจะช่วยให้ผู้ออกแบบเข้าใจกระบวนการ ออกแบบของเครื่องบินรบไร้คนขับชนิคปีกบินได้ดียิ่งขึ้น

คำหลัก: การออกแบบเครื่องบิน เครื่องบินรบไร้คนขับ ปีกบิน

Abstract

It has been widely agreed that Unmanned Combat Air Vehicle (UCAV) presents many advantages over today manned combat aircraft, and the UCAV is being considered as an effective and affordable weapon system in the near future. The lack of aircrew onboard makes UCAV more desirable for use in the most danger of aerial combat missions which the loss or capture of the aircrew would be unacceptable. Without human onboard, the vehicle can be built, smaller, lighter, cheaper and more efficient. In addition, the UCAV capability as a reusable platform provides a more cost effective attack weapon over the cruise missile. As the flying wing appears to be the most promising configuration due to aerodynamic efficiency and inherently stealthy, the flying wing UCAV is of particular interest for this study.

In this study, an initial sizing and optimization tool is developed for UCAV flying wing design to investigate the influence of design requirements and to explore the characteristic of the flying wing type. The design tool is able to model the cranked wing planform. The simple structure layout consisting of a front spar, a rear spar and ribs forming a wing box is chosen with a weapon bay located underneath a single turbofan engine at the centerline section. The semi-analytical wing mass estimation of a cranked wing planform is developed and employed to provide more accurate wing mass prediction. The aerodynamic loads are evaluated using an analytical code based on the lifting-surface theory. Longitudinal trim and static stability, and lateral and directional stabilities and control sizing are considered in which inboard elevons are used to provide longitudinal and lateral controls, and outboard split-drag rudders are employed for directional control. The LSGRG2 optimizer is integrated into to the design synthesis to obtain the optimum design. The take-off mass is taken as the objective function to be minimized. The tool is employed to investigate the effect of stability requirement on the design. It is found that the required static margin has a significant impact on the design in which relaxing the static margin leads to a smaller and lighter design. The wing sweep of the flying wing design is mainly determined by the stability requirement rather than the typical aerodynamic requirement of the wing drag reduction at high subsonic speed flight. The study also shows that the single leading-edge cranked planform is more efficient for a long range (or larger payload) design due to more aerodynamic efficiency; and flexibility to control the aircraft center of gravity, and static margin of the outboard wing in comparison with the straight leading-edge planform. The design tool can be used effectively for sensitivity study to provide more insight into the design and in turn decision making at the initial design stage.

Keyword: Aircraft design, unmanned combat air vehicle, UCAV, flying wing

Executive Summary

Introduction:

It has been widely agreed that Unmanned Combat Air Vehicle (UCAV) presents many advantages over today manned combat aircraft, and the UCAV is being considered as an effective and affordable weapon system in the near future. The lack of aircrew onboard makes UCAV more desirable for use in the most danger of aerial combat missions which the loss or capture of the aircrew would be unacceptable. Without human onboard, the vehicle can be built more efficient, smaller, lighter and cheaper. In addition, the UCAV capability as a reusable platform provides a more cost effective attack weapon over the cruise missile.

In 1998, the Defense Advance Research Projects Agency (DARPA) and US Air Force proposed UCAV Advanced Technology Demonstration (ATD) program to demonstrate technical feasibility of a UCAV system. The operational UCAV system is envisioned as an integrated part to support the existing manned strike packages in 2010. In the UK, the Defence Procurement Agency (DPA) is also considering UCAV as a potential candidate system component of the Future Offensive Air System (FOAS) program for the Tornado GR4 replacement in 2017. Several design concepts have been proposed but mostly pointed to the tailless or flying wing design. This is mainly because the flying wing is aerodynamically efficient and inherently stealthy which is a very important feature for performing the dangerous mission such as the Suppression of Enemy Air Defense (SEAD) and deep strike missions to destroy sophisticated enemy air defenses ensuring air superiority. As the flying wing appears to be the most promising configuration, the flying wing UCAV is of particular interest for this study.

The objective of this study is to develop a new initial design and optimization tool for sizing UCAV flying wing based on the design tool developed by Watjatrakul [16]. The tool will be able to model the cranked wing planform. A new internal packaging will be introduced. A wing mass estimation method for the cranked wing planform will be developed to provide more accurate prediction. The aerodynamic module originally using the vortex lattice code will be replaced with the aerodynamic code using lifting-surface theory to provide more robustness and reduce computational time during optimization process. Trim, stability and control sizing will be considered, and included in the optimization process. With the more complete and accurate tool, the characteristics of the flying wing UCAV can be explored in more detail and accuracy.

Program Development and Structure:

The complex nature of the aircraft design problem is mainly due to multidisciplinary interaction involving a large numbers of variables and constraints which can lead to many feasible design solutions for a given set of requirements. To achieve the optimum design, the Multivariate Optimization method —the integration of a numerical optimization into the design synthesis— is employed to tackle the design problem in this

study. The MVO is a single-level optimization approach consisting of two main parts: the design synthesis and optimization (or optimizer). The design synthesis of flying wing UCAV consists of design disciplines and their interactions, i.e. configuration and packaging, mass estimation, aerodynamics, propulsion, performance, and stability and control.

The formulation of MVO begins with identifying: a set of design variables, the objective function to be minimized (optimized) and constraint functions to be satisfied. Design variables are any selected variables, such as wing geometry, that describe the problem and will be altered by the optimizer to obtain the optimum solution. The MVO also includes a number of variables which are fixed from the outset called the design parameters; for example, number of engines, ultimate load factor and payload. As MVO is capable of handling a large number of design variables and constraints, more details of aircraft configuration can be setup, then detail analyses can be performed leading to more accurate design. More insight into the design problem can be obtained by tradeoff studies that show effects of changing the requirements or design variables on the aircraft. This encourages more rigorous analysis for new aircraft concepts. In this study, the optimization code called LSGRG2 is used as the optimizer within the MVO code for the flying wing UCAV design. LSGRG2 uses Generalized Reduced Gradient (GRG) algorithm to solve large-sparse nonlinear problems.

Configuration and Packaging:

As the flying wing appears to be the most promising configuration due to aerodynamic efficiency and stealthy advantage, several designs of flying wing UCAV have been purposed. In late 2004, the Defense Advanced Research Projects Agency (DARPA) awarded Boeing and Northrop Grumman the contacts for construction of Boeing X-45C and Northrop X-47B with larger payload and longer range (see Fig. 3.1). The flight testing of both vehicles is expected to commence in late 2007.

In this study, two designs of flying wing UCAV similar to Boeing X-45C and Northrop X-47B are investigated -the straight leading-edge planform called AU design and the single leading-edge cranked planform called NU design (see Fig. 3.2). Both designs have a similar internal packaging. The simple structure layout consisting of a front spar, a rear spar and ribs forming a wing box is employed. The user enables to specify location of both spars as a constant fraction of local chord. Airfoil data can be given at center, kink and tip sections. The center weapon bay located underneath a single turbofan engine arrangement is chosen in order to minimize the planform area and weight. The user provides the weapon mass and its bay dimension. The engine size and mass are calculated from the maximum required thrust through the thrust scale factor of the datum engine. Tricycle landing gear layout is employed. Landing gear length is calculated to allow for the taildown angle, and tyre size is estimated from the gear load and tyre pressure. The landing gear bay is then determined from the gear dimensions. Avionics and communication system are placed above and beside the nose gear bay. A fuel tank on the semi-span wing is placed inboard next to the main gear bay to control the aircraft center of gravity, and the fuel mass and volume are calculated according to the mission fuel required. Structural clearances between all bays are specified to ensure

practical design. The thickness at the center section is examined to ensure that the components can be accommodated inside the basic airfoil shape to provide smooth contour for stealthy and aerodynamic design. Inboard eleveons are employed for pitch and roll controls; and split-drag rudders are located outboard for yaw control. The optimizer has authority to adjust the planform parameters, and to relocate internal components to achieve the optimum design.

Mass Estimation:

In this study, the aircraft takeoff mass was selected as the objective function to be minimized. A wing mass estimation for the cranked wing planform was developed based on the semi-analytical approaches and presented in details in Appendix A. The structural mass is divided into two parts: the primary box structure and secondary structure. The primary box consists of upper and lower skins, a front and a rear spar and ribs which carry aerodynamic and inertia loads resulting in shear, bending and torsion. The secondary structure comprises fixed leading-edge and trailing-edge structure, high-lift devices and control surfaces. The penalty mass due to attachments and cutouts is added providing the total wing structural mass. The method was then simplified for the single cranked planform (see Section 3.1). All other aircraft component masses are based on the empirical methods expressed in details in Watjatrakul [16].

Aerodynamic Loads:

In this study, the aerodynamic code based on the lifting-surface theory [27] was integrated as a subprogram into the aircraft design code. The spanwise lift of a wing is due to the contributions of angle of attack, airfoil camber, wing twist and control surface deflection.

The total drag coefficient of the wing consists of the drag coefficient of the basic wing and increment in drag coefficient due to control deflection. Drag coefficient of the basic wing is divided into two components: a drag component that is independent of lift and a lift-dependent drag component. In this study, the equivalent wing planform was used to estimate the cranked wing drag coefficient, and the empirical drag prediction [21] was employed (see Section 3.3.2).

The drag increment at zero lift due to plain trailing-edge device deflection was estimated based on the empirical method [24]. The method evaluates drag increment due to full span flap deflection, and the conversion factor [25] was used for part-span flap correction. In this study, plain trailing-edge device type was employed as inboard elevons functioning as both elevator and aileron. The code to estimate drag increment due to full span flap deflection [24] was modified and integrated into the aircraft sizing code as a subprogram.

The empirical method [26] was used to estimate drag increment at zero lift due to split trailing-edge device deflection (see Fig. 3.7). The method evaluates drag increment due to full span flap deflection, and the conversion factor [24] was used for part-span flap

correction. In this study, the drag due to split flap provided the split-drag rudder effect for the directional control. The numerous empirical data of split-flap drag were put into matrices, and Lagrange interpolation method was employed to find the associated data according to the design parameters.

Propulsion:

The engine sizing is evaluated according to the design performance through the scaling factor SF on the datum (nominal) engine. This statistical method, although rather approximate, generally gives accurate results as long as 0.5 < SF < 1.5. In another word, the required engine has characteristics close to the selected datum engine (see Section 3.4).

In this study, the F404-GE-100D propelled Boeing X-45C and F100-PW-220E driven Northrop X-47B were chosen as the datum engines for the AU and NU designs, respectively.

Mission and Point Performances:

The parameter being calculated in the mission analysis is the amount of fuel required to perform the specified mission. Up to 30 combinations of engine run, takeoff, climb and accelerate, cruise, manoeuvre, weapon drop, loiter, landing and taxi phases can be evaluated (see Table 3.2). Aircraft mass at the end of each mission phase is used as the starting mass of the consecutive phase. The mission fuel mass is checked against the fuel mass obtained from the fuel fraction to ensure the consistency of the fuel estimation.

The point performance of the synthesized aircraft has to be estimated to ensure satisfaction of given performance requirements which are used as design constraints. In this study, the following point performances can be estimated: take-off field length, landing field length, attained turn, sustained turn, time to climb and acceleration, maximum level Mach number and specific excess power. For each point performance, aircraft mass, flight condition and required performance must be specified (see Table 3.3). Up to 10 combinations of these point performances can be evaluated. In this study, the fuel mass estimation and point performance analyses follow the methods given in Watjatrakul [16].

Stability and Control:

- Longitudinal Trim and Stability

The equations of motion during steady flight of the flying wing have been developed (see Section 3.7.1) to evaluate trimmed flight at the design point and required control deflection for maximum trimmed lift coefficient.

At the design point, the aircraft is trimmed or balanced with no control deflection to avoid trimmed drag penalty. The optimizer has authority to adjust the planform parameters, and to relocate internal components to achieve the required static margin without control deflection. For high attitude trim such as approach landing and maneuvering, the maximum trimmed lift coefficient is required. In general, the maximum trimmed lift coefficient with control deflection is said to be achieved when the wing lift coefficient of any spanwise section reaches its local maximum airfoil lift coefficient with control deflection. Therefore, by gradually increasing the angle of attack, the stall angle and the maximum trimmed lift including the required control deflection can then be obtained. However, this process will required considerable amount of time for evaluation, particularly involving with optimization process. In this study the stall angle of attack with elevon deflection is assumed conservatively to occur at 12°, then the maximum trimmed lift coefficient and elevon deflection to trim (elevator function) are obtained from the equations of motion. The elevon deflection to trim must not be greater than a half of the specified maximum angle to allow for aileron functioning.

The static margin SM is a crucial requirement for flying wing design. The aircraft is statically stable if SM is positive; neutrally stable if SM is equal to zero; and unstable if SM is negative. The optimizer allows relocating the internal components and changing the wing planform to meet the specified static margin requirement. The effect of required degree of stability on the design of the aircraft was investigated and discussed later.

- Take-off Rotation Control Power

In this study, the rotation at takeoff is also used as a criterion for sizing the inboard elevons in part of elevator function to ensure enough control power for takeoff. The equations of motion during takeoff ground roll have been developed (see Section 3.7.3). The requirement used here is that the aircraft must be able to lift the nose wheel off the ground at a rotation speed of 1.1 of the stall speed in the take-off configuration.

- Lateral and Directional Stability and Control

The lateral stability of the aircraft can be assured by $C_{L_{\beta}} < 0$ where $C_{L_{\beta}}$ is the change in rolling moment coefficient of the aircraft due to sideslip angle β . The sweepback angle and dihedral of the wing provide such the lateral stability. The wing planform contribution to the rolling moment derivative due to sideslip is obtained from the empirical method [28]. The method can be applicable to various wing planforms through the use of the equivalent wing planform concept. The lateral or roll control is provided with elevons functioning as ailerons. In this study, the elevon size for roll control is determined by the requirement to maintain wing level in crosswind. The rolling moment due to elevon deflection, obtained from aerodynamic module, is used to counterbalance the rolling moment due to sideslip (see Section 3.7.4).

The directional stability of the aircraft can be assured by $C_{n_{\beta}} > 0$ where $C_{n_{\beta}}$ is the change in the yawing moment coefficient of the aircraft due to sideslip angle. The

sweepback angle provides such the directional stability. The outboard split-drag rudders are employed for the directional control for holding a zero sideslip angle. The size of rudder is determined base on the worse-case condition during landing and take-off in a crosswind ratio of 0.2 and sideslip angle of $\beta = 12^{\circ}$. The yawing moment due to the split-drag rudder, obtained from aerodynamic module, is used to compensate the yawing moment due to sideslip.

Case Studies and Discussions:

In this study, the requirements for AU designs are specified as closely as those publicly available for Boeing X-45C. Likewise, the requirements for NU designs are specified as closely as those publicly available for Northrop X-47B. Some mission and all point performances, however, are assumed similarly to typical combat aircraft (see Section 4.1).

There are 14 design variables and 37 constraints for AU design; and 15 design variables and 40 constraints for NU design (see Section 4.2). The takeoff mass is chosen as the objective function. The LSGRG2 optimizer then searches for the optimum solution -the minimum takeoff mass- that satisfies all constraints by altering the design variables. Examples of all input files containing design variables, parameters and constraints, are given in Appendix B.

In this study, ten basic design cases with variation of minimum static margin ranging from 0 to -20 are investigated. Note that the kink station for the basic NU designs is fixed at a fraction of 0.4 of the wing semi-span. In addition, an AU-X case is investigated to study the effects of the NU requirements on the AU configuration; and two NU designs with the kink stations at fractions of 0.5 and 0.6 are also studied, called NU-Ks cases. Symmetrical airfoils are used for all design case with NACA 66-018, 64A010 and 64A008 applied at the center, kink and tip stations, respectively (see Section 4.3).

The optimum values of the design variables and constraints for AU and NU designs are given in Section 4.4. It can be seen that all designs were driven by the static margin constraint at takeoff. Relaxing stability (more negative static margin or unstable) resulted in smaller and lighter aircraft which lead to smaller engines and less fuel required. However, the benefit of mass reduction was decreased as the static margin was further relaxed.

It can be seen that the highly leading-edge sweep was obtained in comparison with the sweep of typical subsonic aircraft. Sweep angle is typically employed to avoid drag rise at high subsonic flight. However, high sweep reduces aerodynamic lift and increases structural weight. The highly swept-wing design, therefore, was driven by the requirement of a large moment arm for pitch stability and control for flying wing design. All structural clearance constraints were all binding to keep minimum size and weight. All equality constraints were active as expected.

For AU designs, the engines were sized mainly based on the thrust required for the attained turn requirement, while the required thrusts for the climb and attained turn requirements were the key design parameters driven the engine size for NU designs. The wing area was determined by the landing requirement. The nose gear was sized to the upper limit load, not greater than 15% of the takeoff weight.

For all design, there were sufficient control powers for the elevons to trim at landing, attained turn and sustained turn; and for rotation at takeoff. All designs were laterally and directionally stable. There were sufficient elevon control power for lateral control, and split-rudder control power for directional control in cross-wind flight. Note that the elevons and split-rudders were not sized to their minimum dimensions. This is due to the constant fraction of chord and span of the elevons and split-rudders specified by the user. For AU designs, the elevons and split-rudders had equal span on the outer wing. For NU designs, the elevon was spanned over the inner wing, and the split-rudder was spanned over the outer wing.

The total mass and component mass were estimated. It can be seen that relaxing static margin has more impact on the takeoff mass of AU designs than that of NU designs. The component center of gravity (CG) and the excursion of center of gravity were calculated. As the aircraft CG location has significant impact on the required static margin, the payload CG and fuel CG were enforced to locate at the operating empty mass CG to avoid CG movement during flight. Therefore, the forward and aft CG limits are identical. A number of internal packaging constraints were imposed to ensure CG consistency. The dimensions of landing gear bay and engine bay were calculated, and then used as design constraints for internal packaging to ensure practical design.

An additional AU design called AU-X was investigated with the same requirement as the NU3 design. It is found that the AU-X design had much larger weight than the NU3 design. This indicated that the single leading-edge cranked planform of NU was more (aerodynamically) efficient than the straight leading-edge planform of AU for longer range or larger aircraft.

Further NU design cases with variation of kink stations called NU-Ks were investigated. It can be seen that the shorter the kink station, the smaller (and lighter) the aircraft. The shorter kink station indicates the longer outer-wing span and larger area. With the larger wing area of the outer wing associated with smaller sweep, the wing planform is more aerodynamically and structurally efficient; and more adaptable to achieve stability requirement leading to lighter and smaller design.

The aerodynamic loads of AU3 and NU3 designs are illustrated (see Figs. 4.1 and 4.2). It can be seen that the total lift coefficient of the basic wing (i.e. wing without control deflection) at the design point is the sum of lift coefficients due to the wing camber, twist and angle of attack of the planform. A slightly bumpy rise occurred at the outboard section of the NU3 basic wing due to the smaller sweep at the outboard wing providing an increase in lift coefficient.

The convergence histories of takeoff mass (the objective function) and static margin constraint of the AU3 design are illustrated (see Figs. 4.3 and 4.4). It can be seen that 46

iterations driven by the LSGRG2 optimizer were required to achieve the optimum design, i.e. minimized takeoff mass. A strong influence of the static margin on the takeoff mass can be clearly seen. The static margin constraint was first satisfied at the 24th iteration in which the takeoff mass was also increased considerably. The takeoff mass was then relatively constant as the static margin was tied to its lower bound.

It was also found that a realistic starting point of the design is generally preferred in order to avoid divergence and to reduce computational time during the optimization process. According to the results obtained from the design tool, the optimum configurations of AU3 and NU3 designs are modeled and shown (see Fig. 4.5 and 4.6). The average computational time to obtain an optimum design was about 180 minutes on Intel Pentium 4, CPU 3.00 GHz and 1.00 GB of RAM.

Conclusions:

An initial design and optimization tool was developed for unmanned flying wing combat aircraft. The tool was used to investigate the influence of design requirements and to explore the characteristic of the flying wing type. The straight leading-edge planform and single leading-edge cranked planform having similar internal packaging can be modeled. According to results obtained from this study, the following conclusions can be made:

- The required static margin had a significant impact on the design in which relaxing the static margin lead to a smaller and lighter design.
- The single leading-edge cranked planform was more efficient for long range (or larger payload) design due to more aerodynamic efficiency and flexibility to control static margin of the outboard wing compared with the straight leadingedge planform. However, the leading-edge cranked planform provides more radar reflecting angles causing the aircraft less stealthy.
- The wing sweep of the flying wing design was mainly determined by the static margin requirement rather than the typical aerodynamic requirement of the drag reduction at high subsonic speed flight.
- The kink station of the planform showed an impact on the design in which smaller kink span, providing greater outboard wing span associated with smaller sweep, lead to a lighter design.
- Although the planforms of AU and NU designs are similar to the Boeing X-45C and Northrop X-47B, the design requirements of X-45C and X-47B are not sufficiently available in public domain. Therefore, the direct comparison to the AU and NU designs cannot be made at this stage.
- It was found that as the design optimization problem involved a large number of design variables, constraints and complicated analysis, the design code became less robust. A realistic starting point of the design was usually required. In

addition, it was found that scaling of the design variables and constraints showed a significant impact on the robustness and convergence of the solution. Therefore, the design variables (and also constraints) should be scaled to have values of the same magnitude to avoid mathematical ill-conditions during optimization process.

Acknowledgements

In performing this research, I have received a great deal of assistance from many individuals and colleagues who have given information and encouragement. In particular, I would like to thank Asst. Prof. Udomkiat Nontakaew at King Monkut's Institute of Technology North Bangkok; and Dr. Howard Smith at Cranfield University for their valuable comments and suggestions. I would also like to acknowledge the Commission on Higher Education (CHE) and the Thailand Research Fund (TRF) for providing financial support in performing this research. Finally, I offer my deepest, personal thanks to my wife and family who have provided encouragement and humor during the time-consuming process of this study.

Contents

บทคัดย่อ				
Abstract				
E	Executive Summary			
A	eknowledgements	xii		
1.	Introduction	1		
2.	Program Development and Structure 2.1. Multivariate Optimization (MVO) 2.2. Optimization Tool	3 3 5		
	Design Syntheses 3.1. Configuration and Packaging 3.2. Mass Estimation 3.2.1. Wing mass estimation 3.3. Aerodynamic Loads 3.3.1. Lift and Pitching Moment Estimation 3.3.2. Drag Estimation 3.4. Propulsion 3.5. Mission Performance 3.6. Point Performance 3.7. Stability and Control 3.7.1. Longitudinal Trim and Static Stability 3.7.2. Trimmed Lift Coefficient 3.7.3. Take-off Rotation Control Power 3.7.4. Lateral and Directional Stability and Control	6 6 9 10 14 14 15 20 22 23 24 24 27 28 31		
4.	Case Studies and Discussions 4.1. Requirements 4.2. Design Variables and Constraints 4.3. Case Studies 4.4. Results and Discussions	33 33 34 37 38		
5.	Conclusions	59		
6.	References	61		

Appendix A:	Development of Semi-analytical Approach for Wing Structural Weight Estimation	63
Appendix B:	Examples of Input Files	95
Appendix C:	Publications 1. Watjatrakul B, Development of Semi-Analytical Approach for Wing Structural Weight Estimation, The Journal of KMITNB, Vol.15, No. 4, Oct-Dec, 2005.	108

1. Introduction

In the last two decades, there has been an increased interest in application of the unmanned aerial vehicle in combat roles [1-14]. Eliminating the loss or capture of aircrews and reducing the cost of operating combat aircraft have driven the interest into a new class of air weapon platform, Unmanned Combat Air Vehicle (UCAV). The UCAV is principally a combat aircraft without pilots onboard. It mostly operates autonomously with preprogrammed computers onboard; however, it will be taken over the mission control by remote operators on ground control station or another aircraft in circumstances when human decision is required; for example, releasing weapons, retargeting or aborting the mission. The lack of human onboard makes the UCAV more desirable for used in most dangerous missions such as "the first day of the war", a high threat environment mission in which the probability of survival is low, or hazardous missions involving chemical warfare. As a reusable platform, UCAV provides a more cost effective attack weapon over a cruise missile, and also reduces the risk of collateral damage. With this versatility, the UCAV provides a wider range of options in the battlefield and would potentially revolutionize the battlefield of the future.

In 1998, the Defense Advance Research Projects Agency (DARPA) and US Air Force proposed UCAV Advanced Technology Demonstration (ATD) program to demonstrate technical feasibility of a UCAV system. The operational UCAV system is envisioned as an integrated part to support the existing manned strike packages in 2010 [13]. In the UK, the Defence Procurement Agency (DPA) is also considering UCAV as a potential candidate system component of the Future Offensive Air System (FOAS) program for the Tornado GR4 replacement in 2017. Several design concepts have been proposed but mostly pointed to the tailless or flying wing design. This is mainly because the flying wing is aerodynamically efficient and inherently stealthy which is a very important feature for conduction the dangerous mission such as the Suppression of Enemy Air Defense (SEAD) and deep strike missions to destroy sophisticated enemy air defenses ensuring air superiority.

It can be seen that UCAV presents many advantages over today manned combat aircraft and is being considered as an effective and affordable weapon system in the near future. However, as the flying wing UCAV is a new vehicle concept, there are several unknowns that need to be explored. This research will focus on the design at the conceptual level of the UCAV vehicle itself, not the operational aspect. As the flying wing appears to be the most promising configuration due to aerodynamic efficiency and stealthy advantage, the flying wing UCAV is of particular interest for investigation. Surprisingly, only few works are found in the public domain concerning the flying wing design and optimization. For example, Whittle [15] conducted a study of enhancement of manned combat aircraft supportability using a flying wing configuration as a case study. Several important features of the flying wing configuration were considered, e.g. packaging, trim longitudinal and lateral stability and control. However, as the purpose of his study was not to investigate characteristics of the flying wing type, most of the analyses were based on simplified semi-empirical method, and the control sizing and stability analyses, the important aspects of the flying wing design, were left outside the optimization loop.

Watjatrakul [16] developed a design and optimization tool and performed the study of a subsonic flying wing UCAV compared with the manned version at the initial design level. The emphasis of the design was on the aerodynamic prediction, trim and longitudinal static stability and control sizing of the vehicle. The vortex lattice code called HASC was used to estimate lift, induced drag and pitching moment coefficients. By this mean, the aerodynamic characteristics of the flying wing obtained are based on the true geometry of the wing rather than semi-empirical methods. A linearization approach was developed to estimate trimmed lift and moment coefficients at an angle of attack, and the maximum trimmed lift coefficient was also estimated for performance analyses and control sizing. The takeoff rotation constraint was used for sizing the longitudinal control surfaces. However, although the aerodynamic module based on the vortex lattice method can model several types of wing planform, the straight tapered wing planform was only considered due to the limitation of the packaging module. In addition, the lateral and directional stability and control were not included. The results obtained from the study show that the unmanned version shows a weight saving compared with the manned version performing the same mission. However, both versions of vehicles with a straight tapered wing planform have a similar size. This is mainly due to the impact of the required static margin constraint resulting a large wing area and span. Therefore, the weight saving is mainly obtained from the removal of the pilot and associated mass and the reduction in the ultimate load factor which also lead to less fuel being required. However, for a flying wing with a different wing planform such as a cranked wing planform, the weight saving benefit of the unmanned version is expected to be higher and the vehicle size should be smaller. These require further investigations.

The objective of this study is to develop a new initial design and optimization tool for UCAV flying wing based on the design tool developed by Watjatrakul [16]. The tool will be able to model the cranked wing planform. A new internal packaging will be introduced. A wing mass estimation method for the cranked wing planform will be developed and employed. The aerodynamic module originally using the vortex lattice code will be replaced with the aerodynamic code using lifting-surface theory [27] to provide more robustness and reduce computational time during optimization process. Lateral and directional stabilities and control sizing will be considered, and included in the optimization process. With the more complete and accurate tool, the characteristics of the flying wing UCAV can be explored in more detail and accuracy.

2. Program Development and Structure

Aircraft design is an engineering process of creating a flying machine to meet certain requirements specified by customers or to explore new designer innovations. The design process is an intellectual activity that is reinforced by intuition developed via experience by paying attention to several designs both successful and unsuccessful in the past; and by design procedures and statistical databases. The complex nature of the aircraft design problem is mainly due to multidisciplinary interaction involving a large numbers of variables and constraints which can lead to many feasible design solutions for a given set of requirements. To achieve the optimum design, the Multivariate Optimization method—the integration of a numerical optimization into the design synthesis— is employed to tackle the design problem in this study.

2.1 Multivariate Optimization

An initial sizing and optimization code based on the Multivariate Optimization (MVO) method was developed and employed to evaluate the flying wing UCAV characteristics in this study. The MVO is a single-level optimization approach consisting of two main parts: the design synthesis and optimization (or optimizer) as illustrated in Fig. 2.1. The design synthesis of UCAV consists of design disciplines and their interactions as shown in Fig. 2.2.

The formulation of MVO begins with identifying: a set of design variables, the objective function to be minimized (optimized) and constraint functions to be satisfied. Design variables are any preselected variables that describe the problem and will be altered by the optimizer to obtain the optimum solution. They can be planform geometries, engine thrust, or stability parameters, for example. The objective function is used as a figure of merit to indicate the optimum solution. In aircraft design problem, the objective function can be takeoff mass or life cycle cost to be minimized; or mission radius to be maximized. Constraint functions are imposed to ensure that the aircraft can meet the specified requirements (e.g. the takeoff field length, cruise speed and sustained turn), and be a realistic design (e.g. fuel volume available and structural clearance constraints). The optimizer then uses a numerical optimization technique to search for the optimum solution that meets all design constraints by adjusting the design variables. The MVO also includes a number of variables which are fixed from the outset called the design parameters; for example, number of engines, ultimate load factor and payload. As MVO is capable of handling a large number of design variables and constraints, more details of aircraft configuration can be setup, then detail analyses can be performed leading to more accurate design. More insight into the design problem can be obtained by tradeoff studies that show effects of changing the requirements or design variables on the aircraft. This encourages more rigorous analysis for new aircraft concepts.

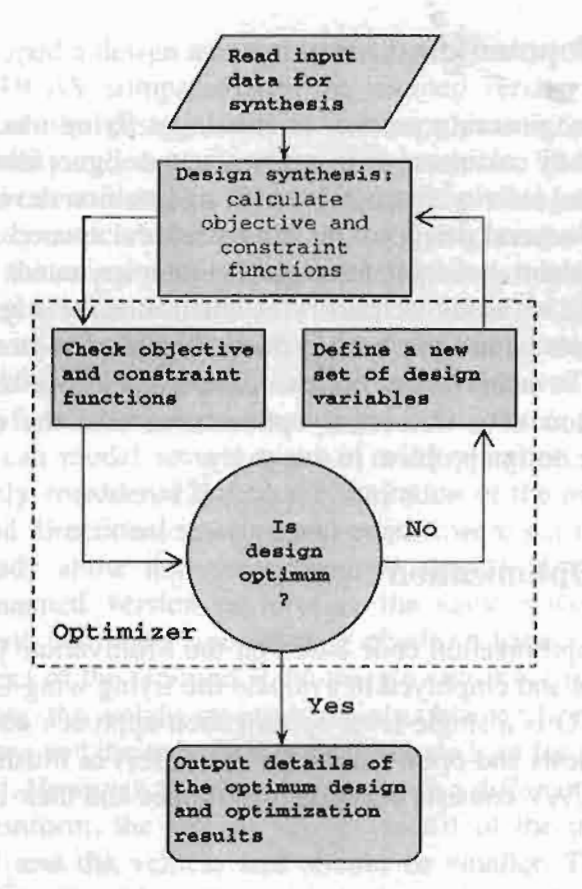


Fig. 2.1 Basic algorithm of the multivariate optimization (MVO).

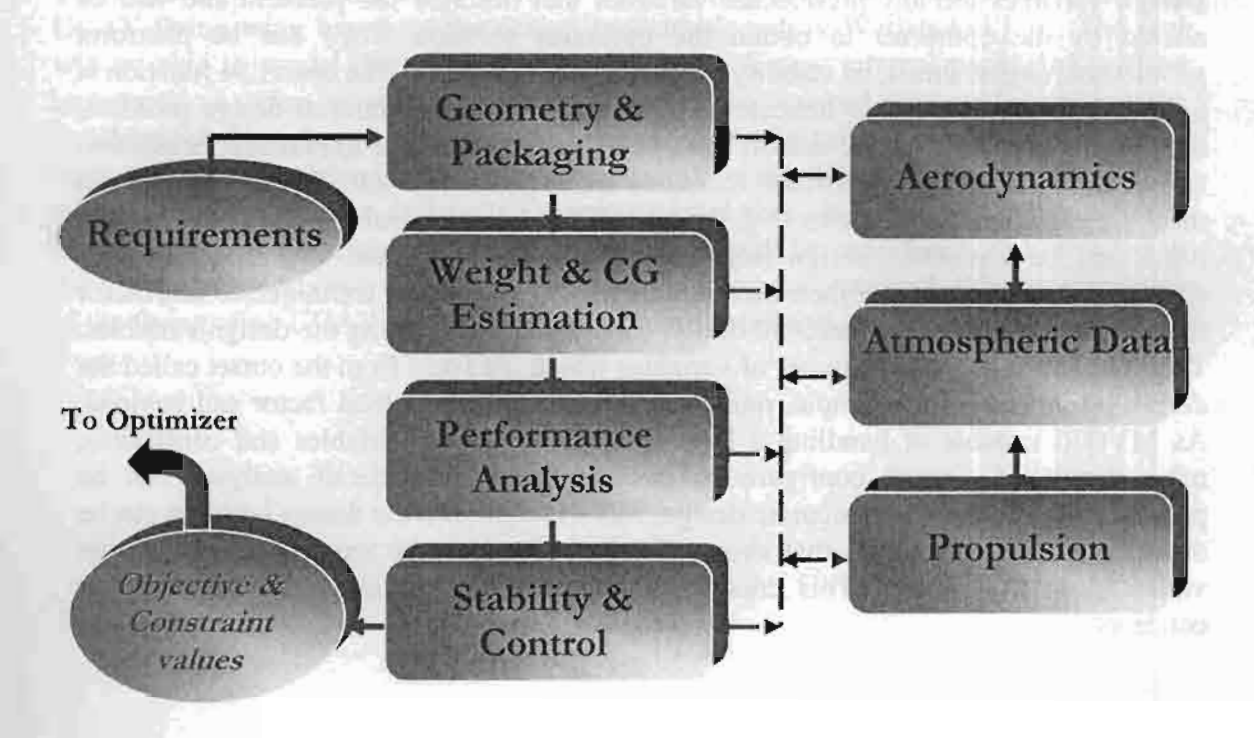


Fig. 2.2 Aircraft design synthesis.

2.2 Optimization Tool

In this study, the optimization code called LSGRG2 [17] is used as the optimizer within the MVO code for UCAV design. LSGRG2 uses Generalized Reduced Gradient (GRG) algorithm to solve large-sparse nonlinear problems of the following form:

Find an n-vector $X = (X_1, X_2, X_3, ..., X_n)$ of Design variables to Minimize: $G_k(x)$ Objective function Subject to: $l(n+i) \le G_i(x) \le u(n+i) \quad i = 1,2,..., m \text{ but } i \ne k \quad \text{Constraint functions} \\ l(i) \le X \le u(i) \qquad i = 1,2,..., n \quad \text{Bound constraints}$

where X is a vector of n design variables, G_i is a vector of m constraint functions and G_k is the objective function to be optimized. The lower bound vector, l, and the upper bound vector, u, are the constraints of the design variables.

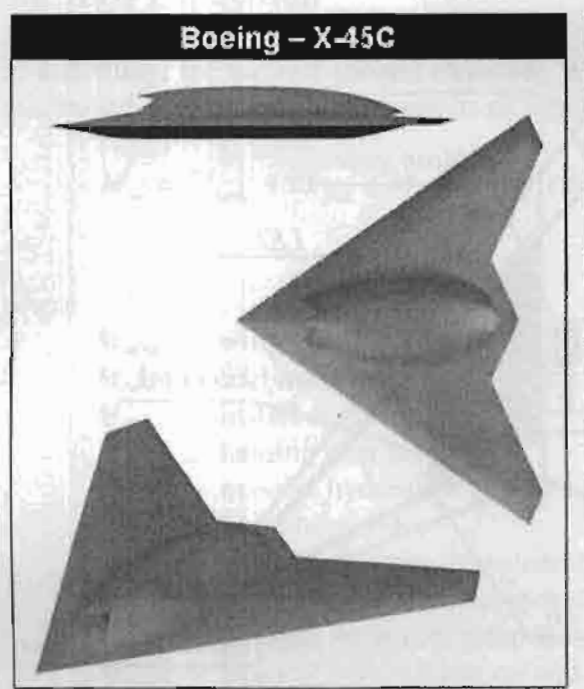
As in other gradient-based methods, LSGRG2 uses gradients of the objective and constraint functions to find a search direction which will move the current design point toward the optimum solution that meets all constraints. A step size is then calculated to provide a step move of the design variables in the search direction. The gradients of the functions with respect to each design variable $(\partial G/\partial X_i)$, if not given, can be estimated automatically using the finite difference method. If the starting point supplied by the user violates the constraints (i.e. outside the feasible region), the optimization phase I is started in order to find a feasible design. If a feasible point is found, the phase II is then started to find the optimum solution. The local optimum is said to be found when the Khun-Tucker conditions are met, or the fractional change in the objective function is less than a specified tolerance. If a feasible point can not be found, the program terminates. A constraint function is said to be active or binding when the design point is lying on the constraint within a specified limit. Details of the LSGRG2 algorithm and implementation can be found in Lasdon [17].

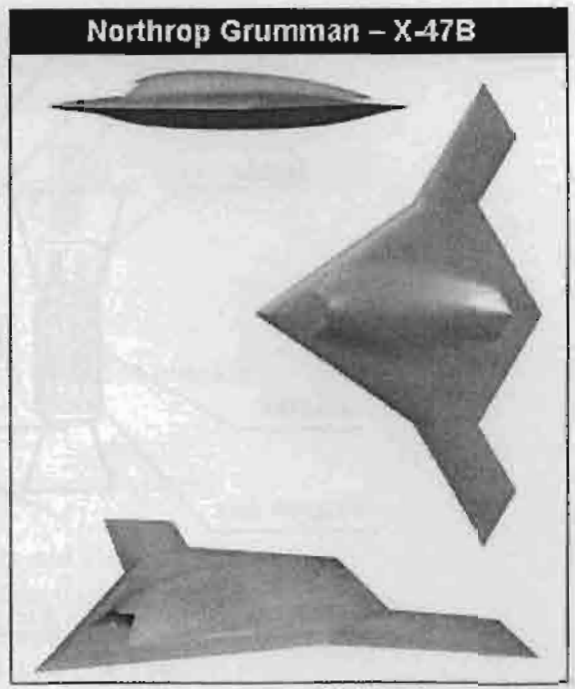
3. Design Syntheses

3.1 Configuration and Packaging

Flying wing configuration appears to be the most promising configuration due to aerodynamic efficiency and stealthy advantage; therefore, the flying wing UCAV is of particular interest for investigation. Aerodynamic superiority of the flying wing is obtained through eliminating non-lift producing components (i.e. fuselage and tail unit) leading to reduction in wetted area, drag and weight. Without the tail unit and with smoothly blended external geometry, the radar cross section of the flying wing is reduced significantly. Several designs of tailless UCAV have been purposed. In late 2004, the Defense Advanced Research Projects Agency (DARPA) awarded Boeing and Northrop Grumman the contacts for construction of Boeing X-45C and Northrop X-47B [14] with larger payload and longer range as shown in Fig. 3.1. The flight testing of both vehicles is expected to commence in late 2007.

In this study, two designs of flying wing UCAV similar to Boeing X-45C and Northrop X-47B are investigated -the straight leading-edge planform called AU design and the single leading-edge cranked planform called NU design- as shown in Fig. 3.2. Both designs have a similar internal packaging. The simple structure layout consisting of a front spar, a rear spar and ribs forming a wing box is employed. The user enables to specify location of both spars as a constant fraction of local chord. Airfoil data can be given at center, kink and tip sections. Leading-edge and trailing-edge control devices with constant chords can be modeled. The center weapon bay located underneath a single turbofan engine arrangement is selected in order to minimize the planform area and weight. The user provides the weapon mass and its bay dimension. The engine size and mass are calculated from the maximum required thrust through the thrust scale factor of the datum engine. Tricycle landing gear layout is employed. The landing gear length is calculated to allow for the taildown angle, and the tyre size is estimated from the gear load and tyre pressure. The landing gear bay is then determined from the gear dimensions. Avionics and communication system are placed above and beside the nose gear bay. A fuel tank on the semi-span wing is placed inboard next to the main gear bay to control the aircraft center of gravity, and the fuel mass and volume are calculated according to the mission fuel required. Structural clearances between all bays are specified to ensure practical design. The thickness at the center section is examined to ensure that the components can be accommodated inside the basic airfoil shape to provide smooth contour for stealthy and aerodynamic design. In this study, inboard eleveons are employed for pitch and roll controls, and split-drag rudders are located outboard for yaw control. The optimizer has authority to adjust the planform parameters, for example, sweep angle, wing span, chord, and span of control device; and to relocate internal components such as engine, weapon bay and landing gear attachments to obtain the optimum design.





Specification	Boeing X-45C	Northrop X-47B
Length	11.9 m (39 ft)	11.6 m (38.2 ft)
Wing span	14.9 m (49.5 ft)	18.9 m (62.1 ft)
Height	1.2 m(4ft)	
Weapons Payload	2040 kg (4500 lb) [2 x GBU-31/B JDAM]	2040 kg (4500 lb) [2 x GBU-31/B JDAM]
Empty Weight	18000 lb	>18000 jb
Gross Weight	16600 kg (36500 lb)	19000 kg (42000 lb)
Speed	Mach 0.8-0.85	Mach 0.8-0.85
Ceiling	12200 m (40000 ft)	>12200 m (40000 ft)
Mission Radius	2400 km (1300 nm)	6500 km Range (3500 nm)
Propulsion	GE: F404-GE-102D turbofan 31 kN (7000 lb)	PW: F100-PW-220E turbofan 105.7 kN (23770 lb)

Fig. 3.1 Characteristics of Boeing X-45 and Northrop X-47B designs [14].

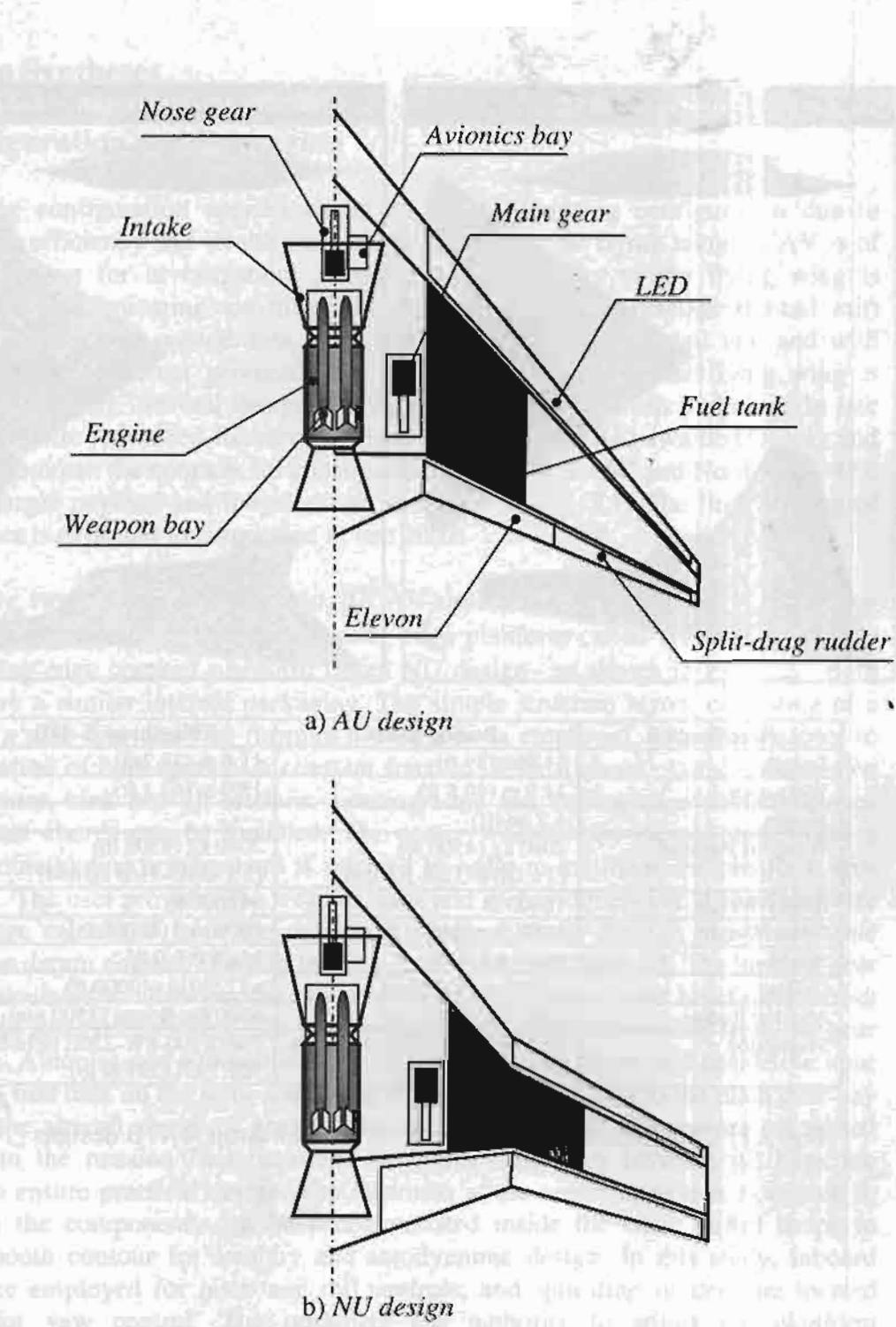


Fig. 3.2 Configuration and packaging of the proposed UCAV designs.

3.2 Mass Estimation

In this study, the aircraft takeoff mass M_{to} was selected as the objective function to be minimized. The takeoff mass consists of the following components:

$$M_{to} = M_{wing} + M_{fuel} + M_{eng} + M_{lg} + M_{hyd} + M_{fur} + M_{avi} + M_{ac} + M_{pay} + M_{comu}$$
(3.1)

where

 M_{wing} is wing structural mass

 M_{fuel} is fuel mass required to perform specified mission

 M_{eng} is install engine mass M_{lg} is landing gear mass

 M_{hyd} is mass of hydraulics and flying control system

 M_{fur} is furnishing mass

 M_{avi} is mass of avionics, instruments and electronics M_{ac} is mass of air conditioning and de-icing system

 M_{pay} is payload mass (i.e. weapon mass)

 M_{comu} is mass of communication and data link system

The M_{pay} and M_{comu} are constant and given by the user according to the design requirement. The other component masses are takeoff mass dependence. In this study, the estimations of M_{eng} , M_{lg} , M_{hyd} , M_{fur} , M_{avi} , and M_{ac} are based on the empirical methods expressed in details in Watjatrakul [16].

The zero fuel mass M_{zf} is defined as

$$M_{zf} = M_{to} - M_{fuel} \tag{3.2}$$

the zero payload mass M_{zp} is

$$M_{vp} = M_{vo} - M_{pay} (3.3)$$

and the operating empty mass M_{OEM} is

$$M_{OEM} = M_{io} - M_{fuel} - M_{pay} \tag{3.4}$$

3.2.1 Wing mass estimation

The wing mass estimation for the cranked wing planform was developed based on the semi-analytical approaches given in Torenbeek [18] and Howe [19, 20], and presented in details in Appendix A. The structural mass is divided into two parts: the primary box structure and secondary structure. The primary box consists of upper and lower skins, a front and a rear spar and ribs which carry aerodynamic and inertia loads resulting in shear, bending and torsion. The secondary structure comprises fixed leading-edge and trailing-edge structure, high-lift devices and control surfaces. The method was then simplified for the single cranked planform. The related simplification is presented in the following.

Material Required Resisting Bending:

The weight of skin materials W_{sk} required for the upper or lower skins to resist bending is obtained from

$$W_{sk} = 2\rho g \int A_{sk}(\mathbf{y}_{s}) \, d\mathbf{y}_{s} \tag{3.5}$$

or

$$W_{sk} = 2\rho g \left(\int_{0}^{y_{k}/\cos \Lambda_{I}} A_{sk}(y_{s}) dy_{s} + \int_{y_{k}/\cos \Lambda_{I}}^{(h/2)/\cos \Lambda_{O}} A_{sk}(y_{s}) dy_{s} \right)$$
(3.6)

where ρg is the material specific weight, $A_{sk}(y_s)$ is the equivalent skin cross-sectional area at structural station y_s , Λ is the mid-chord sweep angle, and y_k is the kink station. The ()_l and ()_O denote the properties of the inner and outer wings, respectively.

Define the span fraction as

$$\eta = \frac{y}{h/2} = \frac{y_s \cos \Lambda}{h/2} = \eta_s \tag{3.7}$$

Hence,

$$d\eta = \frac{dy}{h/2} = \frac{\cos \Lambda}{h/2} dy_s \tag{3.8}$$

From Eq. (3.6), we obtain

$$W_{sk} = 2\rho g \left(\frac{b/2}{\cos \Lambda_{I}} \int_{0}^{\eta_{k}} A_{sk}(y_{s}) d\eta + \frac{b/2}{\cos \Lambda_{O}} \int_{\eta_{k}}^{1} A_{sk}(y_{s}) d\eta \right)$$
(3.9)

The equivalent panel cross-sectional area $A_{sk}(y_s)$ is defined as

$$A_{sk}(y_s) = \frac{M(y_s)}{\eta_i t(y_s) \sigma(y_s)}$$
(3.10)

where $M(y_s)$ is the applied bending moment. Therefore, we have

$$W_{sk} = 2\rho g \left(\frac{b/2}{\cos \Lambda_I} \int_0^{\eta_k} \frac{M(\eta)}{\eta_i t(\eta) \sigma(\eta)} d\eta + \frac{b/2}{\cos \Lambda_O} \int_{\eta_i}^{1} \frac{M(\eta)}{\eta_i t(\eta) \sigma(\eta)} d\eta \right)$$
(3.11)

OΓ

$$W_{sk} = \frac{2\rho g}{\eta_t t_E(\eta = 0)} \left(\frac{b/2}{\overline{\sigma}_t \cos \Lambda_t} \int_0^{\eta_k} \frac{M(\eta)}{t(\eta)/t_E(\eta = 0)} d\eta + \frac{b/2}{\overline{\sigma}_o \cos \Lambda_o} \int_{\eta_k}^{1} \frac{M(\eta)}{t(\eta)/t_E(\eta = 0)} d\eta \right)$$
(3.12)

where $\bar{t}_R = t(\eta)/t_E(\eta=0) \cong 0.78$ for a typical wing design. The thickness at the wing center chord t_E is the thickness obtained form the equivalent wing center chord representing the true wing geometry. The $\bar{\sigma}$ is the allowable tensile stress for the lower skin and allowable compressive for the upper skin, assuming a constant value. Therefore, we obtain

$$W_{sk} = \frac{2\rho g}{\eta_t t_E(\eta = 0) \bar{t}_R} \left(\frac{b/2}{\bar{\sigma}_t \cos \Lambda_t} \int_0^{\eta_t} M(\eta) d\eta + \frac{b/2}{\bar{\sigma}_o \cos \Lambda_o} \int_{\eta_k}^{\eta} M(\eta) d\eta \right)$$
(3.13)

The bending moment due to lift at a spanwise station η is

$$M_{BL}(\eta) = \frac{nW\eta_{cp}}{2} \frac{b/2}{\cos \Lambda} I_{I}(\eta) \tag{3.14}$$

where η_{cp} is the spanwise center of pressure of the equivalent wing planform and

$$I_{1}(\eta) = (1 - \eta)^{3 - 2\lambda + \lambda^{2}}$$
(3.15)

where λ is the taper ratio of the equivalent wing planform.

The weight of skin materials required to resist bending due to lift W_{BL} is then

$$W_{BL} = \frac{2\rho g}{\eta_{i} t_{E}(\eta = 0) \bar{t}_{R}} \frac{nW \eta_{cp}}{2} \left(\frac{1}{\overline{\sigma}_{i}} \left(\frac{b/2}{\cos \Lambda_{i}} \right)^{2} \int_{0}^{\eta_{k}} I_{1}(\eta) d\eta + \frac{1}{\overline{\sigma}_{o}} \left(\frac{b/2}{\cos \Lambda_{o}} \right)^{2} \int_{\eta_{k}}^{1} I_{1}(\eta) d\eta \right)$$
(3.16)

Define the lift bending function as

$$I_{2ML} = \int_{i}^{\sigma} I_{1}(\eta) d\eta = \frac{(1 - \eta_{i})^{(4 - 2\lambda + \lambda^{2})} - (1 - \eta_{o})^{(4 - 2\lambda + \lambda^{2})}}{4 - 2\lambda + \lambda^{2}}$$
(3.17)

where i and o denote the inner and outer stations. The total weight of skin materials required to resist bending due to lift for a single cranked wing planform is then obtained from

$$W_{BL} = \frac{2\rho g}{\eta_{i} t_{\mathcal{E}} (\eta = 0) \overline{t}_{R}} \frac{nW \eta_{cp}}{2} \left\{ r_{c} \frac{1}{\overline{\sigma}_{I,I}} \left(\frac{b/2}{\cos \Lambda_{I}} \right)^{2} I_{2ML,I} + r_{k} \frac{1}{\overline{\sigma}_{O,I}} \left(\frac{b/2}{\cos \Lambda_{O}} \right)^{2} I_{2ML,O} + r_{c} \frac{1}{\overline{\sigma}_{I,c}} \left(\frac{b/2}{\cos \Lambda_{I}} \right)^{2} I_{2ML,I} + r_{k} \frac{1}{\overline{\sigma}_{O,c}} \left(\frac{b/2}{\cos \Lambda_{O}} \right)^{2} I_{2ML,O} \right\}$$

$$(3.18)$$

where r_k and r_c are bending relief factors at the kink and wing centerline, respectively.

Bending Relief Factor:

The contribution of inertia loads on the bending is accounted by the bending relief factor according to the method given in Howe [20].

- The relief factor due to structural weight

It is assumed that the spanwise center of mass of the inner and outer wing is at about 0.37 of its semi-span. The structural relief factor at the kink station $\Delta r_{vi,k}$ is then obtained as

$$\Delta r_{st,k} = 9 \times \frac{0.37}{2} \times \frac{Q_{s,o}}{2} = 0.833 Q_{s,o}$$
 (3.19)

The structural relief factor at the wing centerline $\Delta r_{st,c}$ is obtained as

$$\Delta r_{u,c} = \left(9 \times \frac{Q_{s,o}}{4} \times (1 - 0.63\beta_k)\right) + \left(9 \times \frac{0.37}{2} \times \frac{Q_{s,i}}{2} \times (1 - \beta_k)\right)$$
(3.20)

and

$$\beta_k = \frac{b_o}{b} = \frac{b_o}{b_i + b_o} \tag{3.21}$$

where $Q_{S,o}$ and $Q_{S,i}$ are the ratios of structural weight of the outer wing and the inner wing to the takeoff weight W_{to} , respectively. β_k is the ratio of the outer wing span b_o to the total wing span b_i and b_i is the inner wing span.

- The relief factor due to fuel weight

The relief factor due to fuel weight at the kink station $\Delta r_{f,k}$ is obtained as

$$\Delta r_{f,k} = 9 \times \frac{\overline{\eta}_{f,o}}{2} \times Q_{F,o} \times \frac{W_{fuel}}{2W_{to}}$$
(3.22)

The relief factor due to fuel weight at the wing centerline $\Delta r_{f,c}$ is obtained as

$$\Delta r_{f,c} = \left(9 \times \frac{Q_{F,o}}{2} \times \left(1 - (1 - \overline{\eta}_{f,o})\beta_k\right) \times \frac{W_{fuel}}{2W_{to}}\right) + \left(9 \times Q_{F,i} \times \left(\overline{\eta}_{f,i}(1 - \beta_k)\right) \times \frac{W_{fuel}}{2W_{to}}\right)$$
(3.23)

and

$$\overline{\eta}_{i,i} = 2\overline{y}_{i,i}/b_i; \qquad \qquad \overline{\eta}_{i,o} = 2\overline{y}_{i,o}/b_o \qquad (3.24)$$

where $Q_{F,o}$ and $Q_{F,i}$ are the ratio of fuel weight in the outer wing and inner wing to the total fuel weight W_{fuel} , respectively. $\overline{y}_{f,i}$ is the spanwise center of mass of inner fuel tank out from the wing centerline, and $\overline{y}_{f,o}$ is the spanwise center of mass of outer fuel tank out from the kink station.

- Total relief factor

The total relief factor due to inertia loads r_k at kink station is then obtained as

$$r_k = 1 - (\Delta r_{s,k} + \Delta r_{f,k}) \tag{3.25}$$

At the wing centerline, the total relief factor r_c is

$$r_c = 1 - (\Delta r_{s,c} + \Delta r_{f,c})$$
(3.26)

3.3 Aerodynamic Loads

3.3.1 Lift and Pitching Moment Estimation

In this study, the aerodynamic code given in ESDU 95010 [27] is integrated as a subprogram into the aircraft design code. The aerodynamic code estimates the spanwise loading of wings with control surfaces based on lifting-surface theory. It is applicable to straight tapered as well as cranked wing planforms. The total lift coefficient C_L and pitching moment coefficient C_M of a given wing planform are given as

$$C_{L} = (C_{L})_{\alpha} + (C_{L})_{C} + (C_{L})_{\tau} + (C_{L})_{\delta}$$
(3.27)

$$C_{M} = (C_{M})_{\alpha} + (C_{M})_{C} + (C_{M})_{T} + (C_{M})_{\delta}$$
(3.28)

where ()_{α} denotes for the contribution of angle of attack, ()_C for airfoil camber, ()_T for wing twist, and ()_{δ} for control surface deflection (see Fig. 3.3). The spanwise loading distribution is then given as

$$C_{\iota\iota\iota}\frac{c}{\overline{c}} = \left(\frac{\alpha}{57.3}\right) a \frac{(C_{\iota\iota})_{\alpha}}{(C_{\iota\iota})_{\alpha}} \frac{c}{\overline{c}} + (C_{\iota\iota\iota})_{c} \frac{c}{\overline{c}} + (C_{\iota\iota\iota})_{\tau} \frac{c}{\overline{c}} + (C_{\iota\iota\iota})_{\delta} \frac{c}{\overline{c}}$$
(3.29)

$$C_{mL} \frac{c}{\overline{c}} = \left(\frac{\alpha}{57.3}\right) a \frac{(C_{mL})_{\alpha}}{(C_L)_{\alpha}} \frac{c}{\overline{c}} + (C_{mL})_{C} \frac{c}{\overline{c}} + (C_{mL})_{T} \frac{c}{\overline{c}} + (C_{mL})_{\delta} \frac{c}{\overline{c}}$$
(3.30)

where a is the lift-curve slope and \bar{c} is the geometric mean chord as shown in Fig. 3.4.

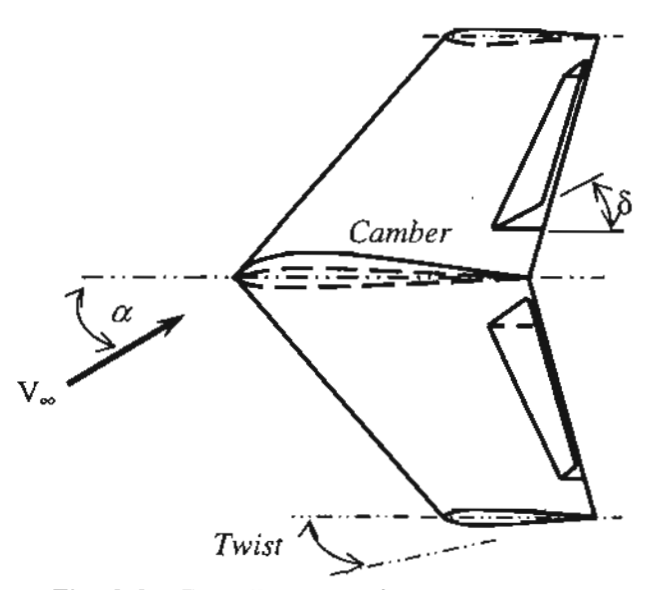


Fig. 3.3 Contributions of aerodynamic loading.

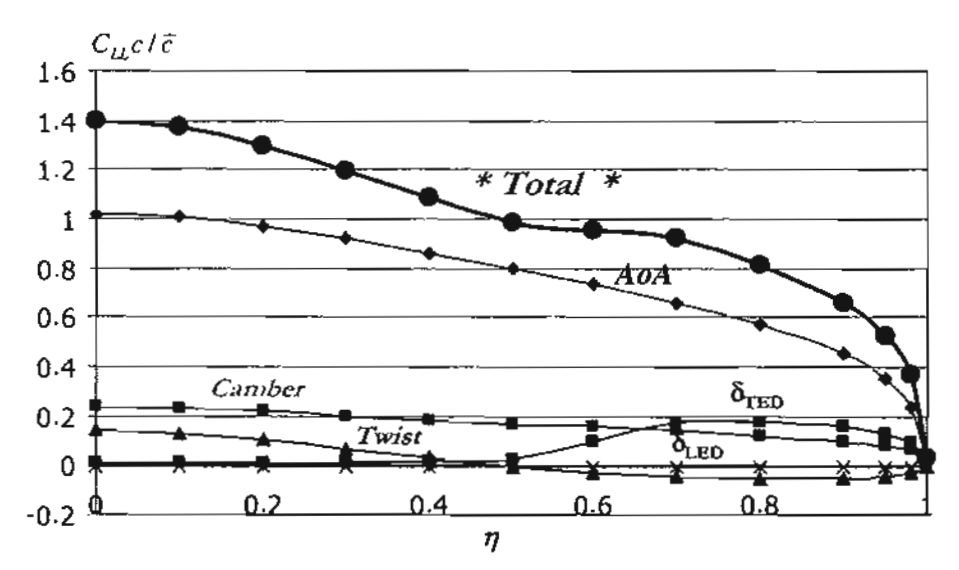


Fig. 3.4 Spanwise loading distribution.

For a cranked wing, the planform is divided into panels. The panels are defined in dimensional terms consisting of the spanwise stations and associated chords of centerline (or root), crank and wing tip. The chordwise coordinates of the wing leading edge at the spanwise stations are obtained through the leading-edge sweep of each panel. At each spanwise station, the camber line ordinates are given in dimensionless from the leading edge to the trailing edge. The twist angles can be specified at each spanwise station assuming linear twist distribution between the stations. The spanwise loadings due to the deflection of plain leading-edge and plain trailing-edge flaps are obtained from specifying flap geometry and deflection on the port and starboard wings.

3.3.2 Drag Estimation

The total drag coefficient of the wing C_D is defined as follows:

$$C_D = C_{Dw} + \Delta C_D \tag{3.31}$$

where C_{Dw} is the drag coefficient of the basic wing and ΔC_D is the increment in drag coefficient due to control deflection.

Basic wing drag:

Drag coefficient of the basic wing C_{Dw} is divided into two components: a drag component that is independent of lift C_{D0w} and a lift-dependent drag component C_{Dlw} .

$$C_{Dw} = C_{D0w} + C_{Dlw} ag{3.32}$$

Several analytical expressions can be used to represent these two drag components. In this study, the simple parabolic drag law was used to represent the drag coefficient of the basic wing that provides accurate prediction within the normal operating range of lift coefficient. As a result,

$$C_{Dw} = C_{D0w} + K_{v}C_{Lw}^{2} \tag{3.33}$$

where K_{ν} is the induced drag factor and C_{Lw} is the lift coefficient of the basic wing. In this study, the equivalent wing planform [23] was employed to estimate the cranked wing drag coefficient, and the empirical drag prediction given in Howe [21] was employed as follows:

$$C_{D0w} = 0.005S^{-0.1} \left[1 - 0.2M + 0.12 \left\{ \frac{M \left(\cos \Lambda_{1/4} \right)^{1/2}}{A_f - t/c} \right\}^{20} \right] R_S T_S (1 - c_{la})$$
 (3.34)

where

S	Wing planform area
M	Operating Mach number
$\Lambda_{1/4}$	Quarter chord sweep (deg)
A_f	Airfoil factor; 0.75-0.93, a higher value for an advanced airfoil
t/c	Wing average thickness to chord ratio
C_{la}	Fraction of laminar flow over the wing chord; 0 for full turbulent flow (recommended)
R_S	Wetted area factor; 2.5 for tailless aircraft
$T_{\mathcal{S}}$	Type factor; 1 for streamline aircraft

and the induced drag factor is

$$K_{v} = \frac{\left(1 + 0.12M^{6}\right)}{\pi A} \left\{ 1 + \frac{0.142 + f(\lambda)A(10t/c)^{0.33}}{\left(\cos \Lambda_{1/4}\right)^{2}} + \frac{0.1}{(4+A)^{0.8}} \right\}$$
(3.35)

where

$$f(\lambda) = 0.005(1 + 1.5(\lambda - 0.6)^2)$$
(3.36)

and λ is the taper ratio of the equivalent wing.

Increment in drag due to control devices ΔC_D :

Plain flap drag

The empirical method given in ESDU 87024 [24] was used to estimate drag increment at zero lift due to plain trailing-edge device deflection. The method evaluates drag increment due to full span flap deflection and the conversion factor given in ESDU Flaps 02.01.07 [25] was used for part-span flap correction. In this study, plain trailing-edge device type is used as inboard elevons functioning as both elevator and aileron.

The total increment in drag coefficient due to full span flap deflection is independent of lift coefficient to a good approximation as shown in Fig. 3.5.

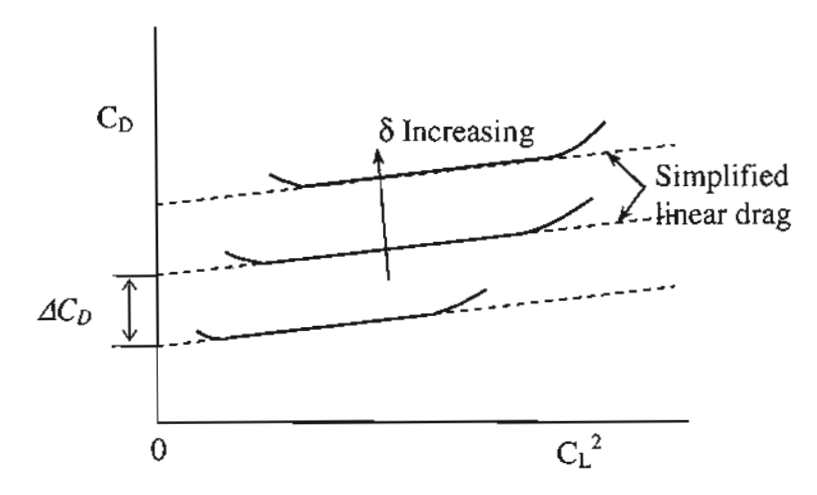


Fig. 3.5 Typical drag characteristics for wing with full-span flap [24].

The code supplied with ESDU 87024 [24] to estimate drag increment due to full span flap deflection was modified and integrated into the aircraft sizing code as a subprogram. The required c, c_f and γ_f (see Fig. 3.6) for each specified airfoil section is treated as the user input.

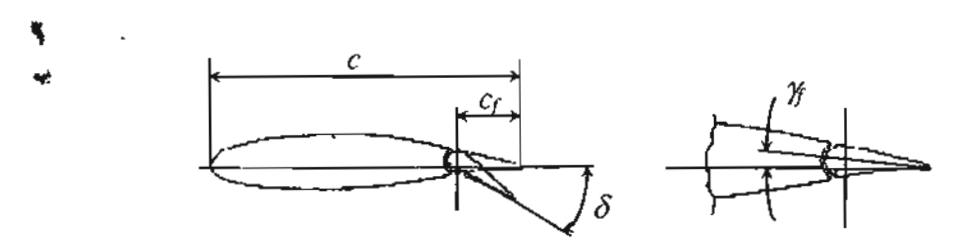


Fig. 3.6 Flap geometry in plane parallel to aircraft plane of symmetry [24].

An empirical method for predicting the zero-lift drag increment due to leading-edge device deflection could not be found. However, Howe [21] suggests that the increment is relatively small; therefore, it is neglected in this study.

Split flap drag

The empirical method given in ESDU 74010 [26] was used to estimate drag increment at zero lift due to split trailing-edge device deflection as shown Fig. 3.7. The method evaluates drag increment due to full span flap deflection and the conversion factor given in ESDU Flaps 02.01.07 [25] was used for part-span flap correction. In this study, the drag due to split flap provides the split-drag rudder effect for the directional control. Similar to plain flap, the total increment in drag coefficient due to full span flap deflection ΔC_D is independent of lift coefficient to a good approximation.

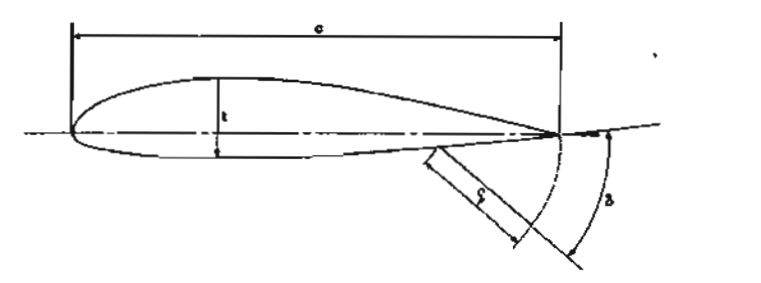


Fig. 3.7 Split flap geometry in plane parallel to aircraft plane of symmetry [26].

The total drag increment due to split flap is given as

$$\Delta C_D = \Delta C_{D0y} \cos \Lambda_{1/4} \tag{3.37}$$

where ΔC_{D0u} is the increment in drag coefficient at zero lift on an unswept wing which is obtained from numerous empirical data given as an example in Fig. 3.8 with values of t/c, c/c, and δ appropriate to a plane parallel to the aircraft plane of symmetry. The data at all intersection points of Fig. 3.8 were put into matrices and Lagrange interpolation method was employed to find ΔC_{D0u} according to the design parameters.

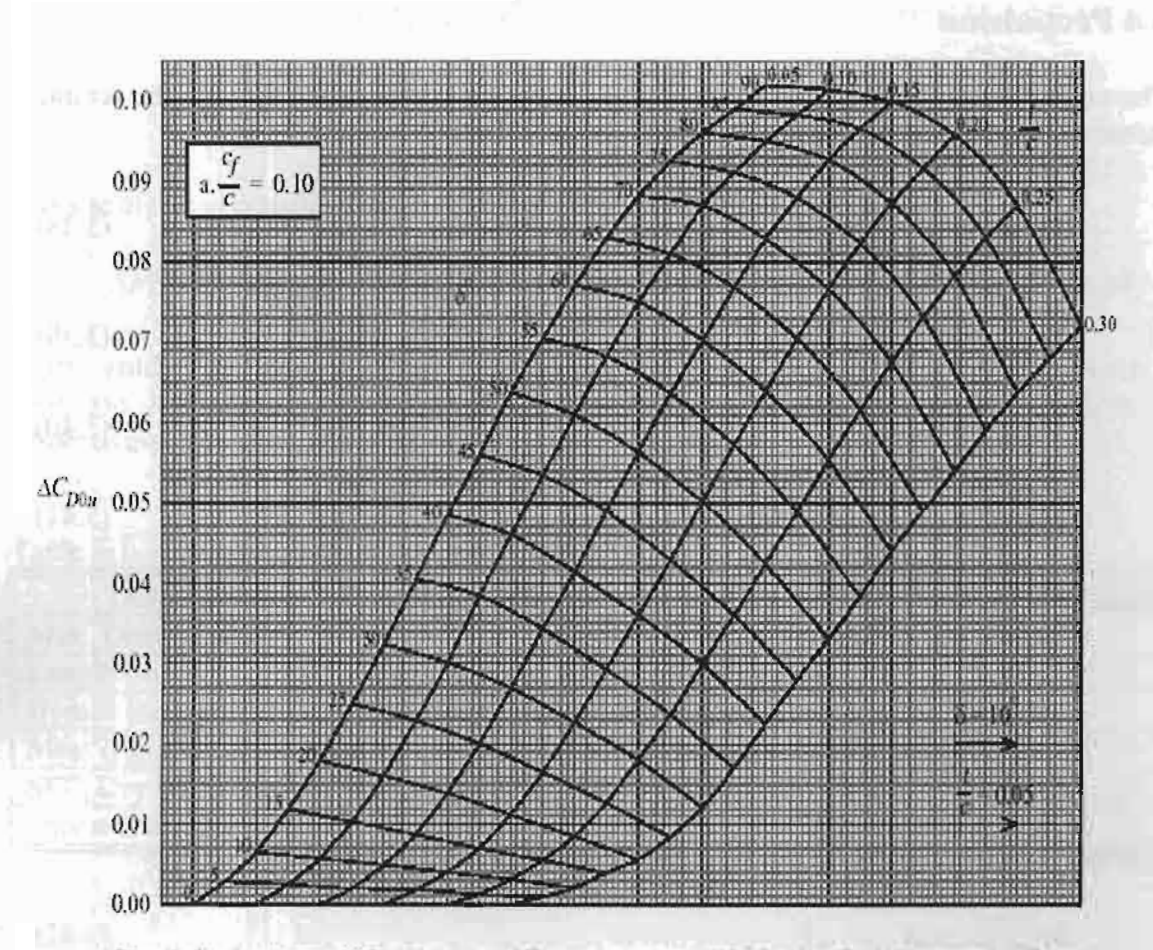


Fig. 3.8 Increment in drag coefficient at zero lift due to full-span split flaps on an unswept wing, $c_f/c = 0.10$ [26].

3.4 Propulsion

The engine sizing is evaluated according to the design performance through the scaling factor SF on the datum (nominal) engine [22] as follows:

$$SF = \frac{\text{Thrust required}}{\text{Thrust of the datum engine}} \quad \text{; at sea level}$$

$$M_{ENG} = M_{ENG,datum} (SF)^{0.4}$$
(3.39)

$$D_{ENG} = D_{ENG,datum} (SF)^{0.5}$$
(3.40)

$$L_{ENG} = L_{ENG,datum}(SF)^{1.1} \tag{3.41}$$

where

 M_{ENG} Uninstalled engine mass D_{ENG} Largest diameter of the required engine L_{ENG} Engine length of the required engine EI Engine mass factor E2 Engine length factor

The total installed engine mass including exhaust and fuel system is defined as:

$$M_{PW} = 1.4M_{ENG} \quad \text{kg} \tag{3.42}$$

This statistical method, although rather approximate, generally gives accurate results as long as 0.5 < SF < 1.5. In another word, the required engine has characteristics close to the selected existing datum engine.

Thrust available at any flight condition for an engine with non-afterburner and low bypass ratio $(B_R < 1)$ is estimated from the method given in Howe [21] as follows:

$$T_0 = (SF)T_{datum} \tag{3.43}$$

$$T = \tau_{eno} T_o \tag{3.44}$$

where

 T_{datum} Sea level static thrust of the selected datum engine (kN) Sea level static thrust of the actual engine (kN) Thrust at any given condition of the actual engine (kN)

 τ_{eng} is a factor depending on the bypass ratio B_R , operating Mach number M_{N_1} and relative density σ as the followings:

$$\begin{split} \tau_{eng} &= \left\{ 1 - \left(0.2 + 0.07 B_R \right) M_N \right\} \sigma^{0.7} &; 0 \le M_N \le 0.4 \\ &= \left\{ \left(0.856 + 0.062 B_R \right) + \left(0.16 - 0.23 B_R \right) M_N \right\} \sigma^{0.7} &; 0.4 < M_N \le 0.9 \\ &= \left\{ \left(1 - 0.145 B_R \right) + \left(0.5 - 0.05 B_R \right) \left(M_N - 0.9 \right) \right\} \sigma^{0.7} &; 0.9 < M_N \le 2.0 \\ &(3.45) \end{split}$$

The specific fuel consumption, SFC, at any flight condition is given as:

$$SFC = SFC_{datum} (1 - 0.15B_R^{0.65}) (1 + 0.28(1 + 0.063B_R^2) M_N) \sigma^{0.08} \qquad \text{N/N/hour} \quad (3.46)$$

In this study, the F404-GE-100D propelled Boeing X-45C and F100-PW-220E driven Northrop X-47B were chosen as the datum engines for the AU and NU designs, respectively. The characteristics of the datum engines are listed in Table 3.1.

Table 3.1 Characteristics of the datum engines

Datum Engine	GE: F404-GE-100D (-102D)	P&W: F100-PW-220E
Max. Diameter (m)	0.882	1.182
Length (m)	2.26	4.986
Bypass Ratio	0.4	0.71
Mass (kg)	826	1430
SFC, Dry (N/N/hr)	0.8	0.73
Thrust SSL, Dry (kN)	48.93	65.25

3.5 Mission Performance

The parameter being calculated in the mission analysis is the amount of fuel required to perform the specified mission. The fuel mass estimation of each mission phase follows the previous work done by Watjatrakul [16]. Up to 30 combinations of mission phases given in Table 3.2 can be evaluated. Aircraft mass at the end of each mission phase is used as the starting mass of the consecutive phase. The mission fuel mass is checked against the fuel mass obtained from the fuel fraction to ensure the consistency of the fuel estimation.

Table 3.2 Mission profile definition

Phase	Code	Altitude	Mach	Datal	Data2	Data3	
Engine run	1	Alt	0.0	Time	0.0	Reheat	
Takeoff	2	Alt	0.0	μ_N	R_{V}	Reheat	
Climb/Accelerate/Descend	3	Altf	Machf	0.0	0.0	Reheat	2
Cruise	4	Alt	Mach	Distance	0.0	Reheat	- 1
Manoeuvre	5	Alt	Mach	Time1 / Deg	Ng	Reheat	•
Weapon drop	6	Alt	Mach	F-Load	0.0	Reheat	
Loiter/CAP	7	Alt	Mach	Time	0.0	Reheat	
Landing	8	Alt	0.0	0.0	0.0	0.0	
End mission	0	0.0	0.0	Fuel Reserve	0.0	0.0	_

Where

Code	Code number given for each point performance
Alt	Flight altitude. (m)
Mach	Mach number
Time	Time duration of the mission segment (minutes)
μ_N	Rolling coefficient for takeoff (0.03 for dry runway)
Distance	Cruise distance (km)
Time1	Combat time, maximum of 10 minutes
Deg	Total degrees of turning, greater than 10 degrees
F-Load	Fraction of total payload to be dropped (0 < F-Load <1)
Fuel Reserve	Fraction of the total fuel to be added
R_V	Ratio of take-off rotation speed to stall speed
Ng	Load factor for manoeuvre (g's)
f	denotes for the final flight condition

3.6 Point Performance

The point performance of the synthesized aircraft has to be estimated to ensure satisfaction of given performance requirements which are used as design constraints. In this study, the following point performances can be estimated: take-off field length, landing field length, attained turn, sustained turn, time to climb and acceleration, maximum level Mach number and specific excess power. For each point performance, aircraft mass, flight condition and required performance must be specified as shown in Table 3.3. Up to 10 combinations of these point performances can be evaluated.

Table 3.3 Point performance definition

Phase	Code	Altitude	Mach	Datal	Data2	Data3	Data4	Data5	Data6
Take-off	1	Alt	0.0	0.0	F-Fuel	F-Load	0.0	0.0	STOG
Attained Turn	2	Alt	Mach	1./2.	F-Fuel	F-Load	0.0	0.0	Ng / (°/s)
Sus. Turn	3	Alt	Mach	1. / 2.	F-Fuel	F-Load	0.0	0.0	Ng / (°/s)
Mach/Speed	4	Alt	Mach	0.0	F-Fuel	F-Load	0.0	0.0	0.0
Accel/Climb	5	Αlti	Mach,	Alt_f	Machf	F-Load	0.0	F-Fuel	Time
Excess Power	6	Alt	Mach	Ng	F-Fuel	F-Load	0.0	0.0	\mathbf{P}_{s}
Landing	0	Alt	0.0	μ _Β	F-Fuel	F-Load	Arrest	0.0	S_{LAND}

Where

Code	Code number given for each point performance
Alt	Flight altitude (m)
Mach	Mach number
Ng	Load factor for manoeuvre (g's)
1. / 2.	Option for specifying turn performance
	1 = load factor; 2 = turn rate
μ_{B}	Braking coefficient (0.4 for dry runway)
F-Fuel	Fraction of take-off fuel carrying $(0 \le F\text{-Fuel} \le 1)$
F-Load	Fraction of total payload carrying (0 ≤ F-Load ≤1)
Arrest	Efficiency of arresting device (0 for none; 1 for high-efficiency)
S_{TOG}	Maximum takeoff ground roll distance (m)
°/s	Turn rate (deg/s)
Time	Time for completing climb or acceleration phase (minutes)
P_s	Specific excess power required. (m/s)
SLAND	Maximum landing ground roll distance (m)
i	denotes for initial flight condition
f	denotes for final flight condition
	Alt Mach Ng 1./2. µB F-Fuel F-Load Arrest STOG °/s Time P _s SLAND

Note that Data 4 is not used in all calculations. It is an option for using afterburner which can be added in further work. The detail analysis of each point performance follows the previous work done by Watjatrakul [16].

3.7 Stability and Control

3.7.1 Longitudinal Trim and Static Stability

Considering an aircraft in steady flight as shown in Fig. 3.9.

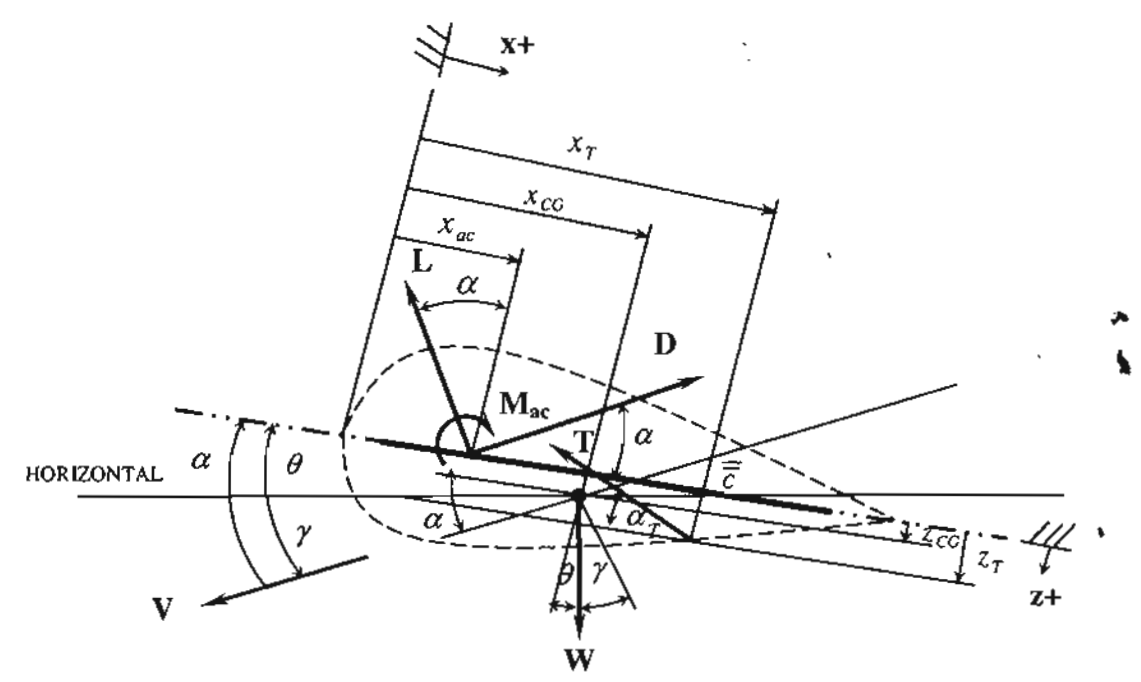


Fig. 3.9 Force system in steady flight.

The equations of motion along and normal to the flight path, respectively, are obtained as

$$D = W \sin \gamma + T \cos(\alpha_T + \alpha) \tag{3.47}$$

$$L + T\sin(\alpha_T + \alpha) = W\cos\gamma \tag{3.48}$$

and the moment about the center of gravity at trim is

$$M_{CG} = 0 = M_{ac} + L\cos\alpha(x_{CG} - x_{ac}) - L\sin\alpha z_{CG} + D\cos\alpha z_{CG} + D\sin\alpha \cdot (x_{CG} - x_{ac}) + T\cos\alpha_T(z_T - z_{CG}) - T\sin\alpha_T(x_T - x_{CG})$$
(3.49)

For level flight, $\gamma = 0$ and $\alpha = \theta$, and

$$C_L = L/(qS);$$
 $C_D = D/(qS);$ $C_M = M/(qS\overline{\overline{c}})$ (3.50)
 $q = \rho V^2/2$

We have

$$C_{L} + \frac{T}{qS}\sin(\alpha_{T} + \alpha) = \frac{W}{qS}$$
(3.51)

$$C_D = \frac{T}{qS}\cos(\alpha_T + \alpha) \tag{3.52}$$

$$C_{M,CG} = 0 = C_{M,ac} + C_L \left[\frac{(x_{CG} - x_{ac})\cos\alpha - z_{CG}\sin\alpha}{\overline{c}} \right]$$

$$+ C_D \left[\frac{z_{CG}\cos\alpha + (x_{CG} - x_{ac})\sin\alpha}{\overline{c}} \right]$$

$$+ C_D \left[\frac{(z_T - z_{CG})\cos\alpha_T - (x_T - x_{CG})\sin\alpha_T}{\overline{c}\cos(\alpha_T + \alpha)} \right]$$
(3.53)

Defining geometry terms as,

$$A = \left[\frac{(x_{CG} - x_{ac})\cos\alpha - z_{CG}\sin\alpha}{\overline{c}} \right]$$

$$B = \left[\frac{z_{CG}\cos\alpha + (x_{CG} - x_{ac})\sin\alpha}{\overline{c}} \right]$$

$$E = \left[\frac{(z_T - z_{CG})\cos\alpha_T - (x_T - x_{CG})\sin\alpha_T}{\overline{c}\cos(\alpha_T + \alpha)} \right]$$
(3.54)

Then, Eq. (3.53) can be written as

$$0 = C_{M,ac} + C_L A + C_D (B + E)$$
 (3.55)

By linearization all forces and moments, we obtain the lift force equation Eq. (3.48) as

$$\begin{bmatrix}
C_{L0w} + \left(\frac{\partial C_L}{\partial \alpha}\right)_w \alpha + \left(\frac{\partial C_L}{\partial \delta}\right)_{hi} \delta_{hi} + \left(\frac{\partial C_L}{\partial \delta}\right)_{tr} \delta_{tr}
\end{bmatrix} + \\
\left[C_{DZw} + K_w \left(C_{Low} + \left(\frac{\partial C_L}{\partial \alpha}\right)_w \alpha\right)^2 + \left(\frac{\partial C_{DZ}}{\partial \delta}\right)_{hi} \delta_{hi} + \left(\frac{\partial C_{DJ}}{\partial \delta}\right)_{hi} \delta_{hi}
+ \left(\frac{\partial C_{DZ}}{\partial \delta}\right)_{tr} \delta_{tr} + \left(\frac{\partial C_{DJ}}{\partial \delta}\right)_{tr} \delta_{tr}
\end{bmatrix} \sin(\alpha_T + \alpha)$$

$$= \frac{W}{qS} \tag{3.56}$$

and the moment equation Eq. (3.55) as

$$0 = C_{M,ac_{w}} + \left(\frac{\partial C_{M,ac}}{\partial \delta}\right)_{hi} \delta_{hi} + \left(\frac{\partial C_{M,ac}}{\partial \delta}\right)_{ty} \delta_{ty}$$

$$+ \left[C_{Lw} + \left(\frac{\partial C_{L}}{\partial \delta}\right)_{hi} \delta_{hi} + \left(\frac{\partial C_{L}}{\partial \delta}\right)_{ty} \delta_{ty}\right] A$$

$$+ \left[\left\{C_{DZw} + K_{w}C_{Lw}^{2}\right\} + \left(\frac{\partial C_{DZ}}{\partial \delta}\right)_{hi} \delta_{hi} + \left(\frac{\partial C_{DI}}{\partial \delta}\right)_{hi} \delta_{hi} + \left(\frac{\partial C_{DZ}}{\partial \delta}\right)_{tr} \delta_{rr} + \left(\frac{\partial C_{DI}}{\partial \delta}\right)_{ty} \delta_{ry}\right] (B + E)$$

$$(3.57)$$

where ()_w denotes for basic wing, ()_{hi} for high-lift devices and ()_{tr} for trim devices. From Eqs. (3.56) and (3.57), the angle of attack (α_{tr}) and control deflection (δ_{tr}) required to trim can be obtained.

At the design point where the aircraft is trimmed or balanced with no control deflection to avoid trimmed drag penalty, we obtain the moment equation, Eq. (3.55), as

$$C_{M,CG} = 0 = C_{M,ac_w} + C_{Lw}A + C_{Dw}(B+E)$$
(3.58)

In addition, the α_{tr} is normally small. Therefore, the lift equation Eq. (3.51) is then

$$C_{t,w} = C_{L0w} + \left(\frac{\partial C_L}{\partial \alpha}\right)_w \alpha_{tr} = \frac{W}{qS}$$
(3.59)

According to the aerodynamic module employed in this study, the lift coefficient of the basic wing is represented as

$$C_{Lw} = C_{LA} + C_{LC} + C_{LT} = \left(\frac{\partial C_L}{\partial \alpha}\right)_{w} \alpha_{tr} + C_{LC} + C_{LT}$$
(3.60)

where C_{LA} is the lift contribution due to angle of attack, C_{LC} is due to airfoil camber and C_{LT} is due to twist. The airfoil camber and wing twist are given and fixed; hence, C_{LC} , C_{LT} and C_{M,ac_w} are constant. The required C_{Lw} is then obtained from the lift equation Eqs. (3.59) and (3.60) corresponding to the trim angle. The location of the center of gravity required to trim x_{CG} is then obtained from the moment equation. The optimizer allows relocating the internal components and changing the wing planform to meet the trimmed flight condition.

The static margin is obtained from

Static Margin
$$(SM) = \frac{x_{ac} - x_{CG}}{\overline{c}}$$
 (3.61)

The aircraft is statically stable if SM is positive ($x_{CG} < x_{ac}$), neutrally stable if SM is equal to zero ($x_{CG} = x_{ac}$) and unstable if SM is negative ($x_{CG} > x_{ac}$). The optimizer allows

relocating the internal components and changing the wing planform to meet the specified static margin requirement. The effect of required degree of stability on the design of the aircraft will be investigated and discussed later.

3.7.2 Trimmed Lift Coefficient

For a given center of gravity position, the trimmed lift coefficient and control deflection to trim at an angle of attack can be calculated by Eq. (3.57). The control derivatives are calculated from the aerodynamic module. In general, the maximum trimmed lift coefficient with control deflection is said to be achieved when the wing lift coefficient of any spanwise section reaches its local maximum airfoil lift coefficient with control deflection. Therefore, by gradually increasing the angle of attack, the stall angle and the maximum trimmed lift including the required control deflection can then be obtained. However, this process will required considerable amount of time for evaluation, particularly involving with optimization process. In this study the stall angle of attack with elevon deflection is assumed conservatively to occur at 12°, then the maximum trimmed lift coefficient and elevon deflection to trim are obtained from the moment equation Eq. (3.57).

3.7.3 Take-off Rotation Control Power

The aircraft, at least, must have enough control power for takeoff if it is able to fly at all. Therefore, the rotation at takeoff is the minimum and crucial requirement for sizing control surfaces. In this study, it is used as a criterion for sizing the inboard elevons in part of elevator function. The requirement used here is that the aircraft must be able to lift the nose wheel off the ground at a rotation speed of 1.1 of the stall speed in the takeoff configuration.

Considering the forces acting on the aircraft during take-off ground roll as shown in Fig. 3.10.

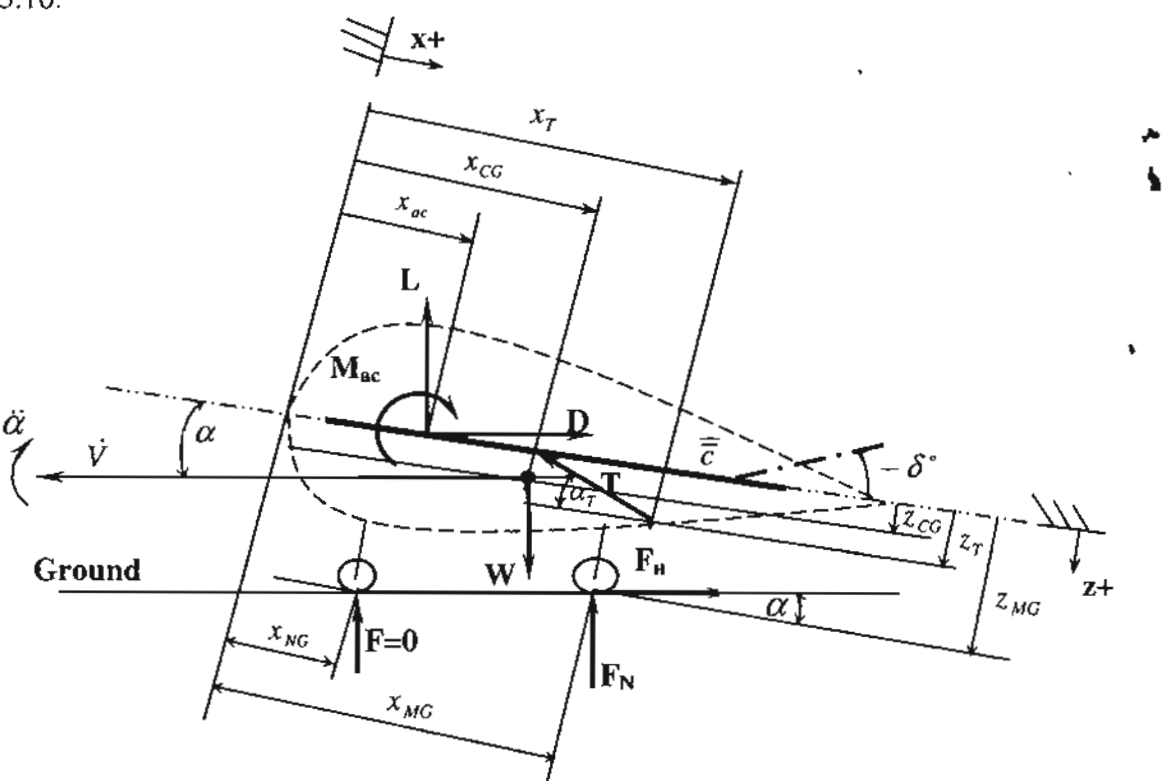


Fig. 3.10 Force system during take-off ground roll.

The forces acting on the aircraft normal and parallel to the flight path, respectively, are

$$L + T\sin(\alpha_T + \alpha) + F_N - W = 0 \tag{3.62}$$

$$T\cos(\alpha_{\Upsilon} + \alpha) - D - F_{H} = \frac{W}{g}\dot{V}$$
(3.63)

As

$$F_H = \mu F_N \tag{3.64}$$

Where μ is the runway friction coefficient; therefore,

$$T\cos(\alpha_T + \alpha) - qSC_D - \mu(W - qSC_L - T\sin(\alpha_T - \alpha)) = \frac{W}{g} \frac{\Delta V}{\Delta t}$$
 (3.65)

The moment around the center of gravity can be written as

$$M_{CG} = I_{CG}\ddot{\alpha} = M_{ac} + L[(x_{CG} - x_{ac})\cos\alpha - z_{CG}\sin\alpha] + D[z_{CG}\cos\alpha + (x_{CG} - x_{ac})\sin\alpha] + T[(z_T - z_{CG})\cos\alpha_T - (x_T - x_{CG})\sin\alpha_T] - F_H[(x_{MG} - x_{CG})\sin\alpha + (z_{MG} - z_{CG})\cos\alpha] + F_N[(z_{MG} - z_{CG})\sin\alpha - (x_{MG} - x_{CG})\cos\alpha]$$
(3.66)

where I_{CG} is the moment of inertia about the pitch axis. Defining geometry terms as

$$A = (x_{CG} - x_{ac})\cos\alpha - z_{CG}\sin\alpha$$

$$B = z_{CG}\cos\alpha + (x_{CG} - x_{ac})\sin\alpha$$

$$E = (z_T - z_{CG})\cos\alpha_T - (x_T - x_{CG})\sin\alpha_T$$

$$G = (z_{MG} - z_{CG})\sin\alpha - (x_{MG} - x_{CG})\cos\alpha$$

$$-\mu((x_{MG} - x_{CG})\sin\alpha + (z_{MG} - z_{CG})\cos\alpha)$$
(3.67)

Then we obtain

$$I_{CG}\ddot{\alpha} = M_{WC} + LA + DB + TE + F_{NG}$$
 (3.68)

By substituting Eqs. (3.62) and (3.63) into (3.68), we have

$$I_{CG}\ddot{\alpha} = qS(\overline{c}C_{M,ac} + C_LA + C_DB - C_LG) + TE + (W - T\sin(\alpha_T + \alpha))G$$
(3.69)

OF 1

$$I_{CG}\ddot{\alpha} = qS \left[\overline{c} \left(C_{M,acw} + \left(\frac{\partial C_{M,ac}}{\partial \delta} \right)_{hi} \delta_{hi} + \left(\frac{\partial C_{M,ac}}{\partial \delta} \right)_{tr} \delta_{tr} \right) \right.$$

$$\left. + (A - G) \left(C_{Lw} + \left(\frac{\partial C_{L}}{\partial \delta} \right)_{hi} \delta_{hi} + \left(\frac{\partial C_{L}}{\partial \delta} \right)_{tr} \delta_{tr} \right) \right.$$

$$\left. + B \left(C_{DZw} + K_{w} C_{Lw}^{2} + \left(\frac{\partial C_{DZ}}{\partial \delta} \right)_{hi} \delta_{hi} + \left(\frac{\partial C_{Di}}{\partial \delta} \right)_{hi} \delta_{hi} + \left(\frac{\partial C_{DZ}}{\partial \delta} \right)_{tr} \delta_{tr} + \left(\frac{\partial C_{Di}}{\partial \delta} \right)_{tr} \delta_{tr} \right] \right.$$

$$\left. + TE + (W - T \sin(\alpha_{T} + \alpha))G \right. \tag{3.70}$$

The stall speed at takeoff is given as

$$V_{S,w} = \sqrt{\frac{2W}{\rho SC_{L \max, lo}}} \tag{3.71}$$

where W is the take-off weight and $C_{Lmax,to}$ is the maximum trimmed lift coefficient at take-off condition. As the aircraft is required to start rotating at 1.1 of stall speed, V_{Sto} ; therefore, the rotation speed, V_R , can be obtained as

$$V_{R} = 1.1 V_{Sm}$$
 (3.72)

As at the start of rotation, $\ddot{\alpha} = 0$; therefore, the control deflection angle $\delta_r = \delta_R$ required to rotate the aircraft at V_R can be calculated by setting Eq. (3.70) equal to zero, and all derivatives are obtained from the aerodynamic module. Note that α is an aircraft setting angle for the take-off ground run. After the nose wheel has lifted off, the aircraft continues to rotate at constant δ_R setting until it lifts off the ground. Note that the elevon deflection for rotation δ_R functioning as elevator must be less than half of the maximum allowable deflection in order to allow for aileron function.

3.7.4 Lateral and Directional Stability and Control

Lateral stability can be achieved by

$$C_{L_{\bullet}} < 0 \tag{3.73}$$

where $C_{L_{\beta}}$ is the change in rolling moment coefficient of the aircraft due to sideslip angle β . The sweepback angle and dihedral of the wing provide such the lateral stability. The wing planform contribution to the rolling moment derivative due to sideslip $C_{L_{\beta}}$ is given in ESDU 80033 [28] is considered to consist of the contribution of the planform independent of wing sweepback and that of wing sweepback as

$$C_{L_{\beta}} = \left[C_{L_{\beta}} \right]_{0} + \left[C_{L_{\beta}} \right]_{\Lambda_{1,1}} \tag{3.74}$$

The contribution due to sweepback is

$$-\left[C_{L\beta}\right]_{\Lambda 1/2}/C_{Lw} = \frac{1}{2}\eta_{cp} \tan \Lambda_{1/2} f(\overline{A})$$
 (3.75)

where

$$f(\overline{A}) = \frac{2 + (4 + \overline{A}^2)^{1/2}}{2 + (4 + \overline{A}^2/4)^{1/2}} \left(1 - \frac{\overline{A}^2/8}{4 + \overline{A}^2/4 + 2(4 + \overline{A}^2/4)^{1/2}} \right)$$
(3.76)

$$\overline{A} = A \sec \Lambda_{1/2} \tag{3.77}$$

$$\tan(\Lambda_{1/2}) = \tan(\Lambda_{1/4}) - \frac{1}{4} \left(\frac{1 - \lambda}{1 + \lambda} \right) \tag{3.78}$$

The contribution of the wing planform without sweepback is

$$-\left[C_{L\beta}\right]_{0}/C_{Lw} = \frac{f_{1}(\lambda)}{A} - f_{2}(\lambda) \tag{3.79}$$

$$f_1(\lambda) = 0.25 + 0.79\lambda - 0.34\lambda^2$$

$$f_2(\lambda) = 0.05 + 0.08\lambda - 0.04\lambda^2$$
(3.80)

The method can be applicable to various wing planforms through the use of the equivalent wing planform concept.

The lateral or roll control is provided with elevons functioning as ailerons. The elevon size for roll control is determined by the requirement to maintain wing level in crosswind. For the crosswind condition, at equilibrium

$$(C_L)_{roll} = 0 = \beta C_{L_R} + C_{L\delta_a} \delta_a \tag{3.81}$$

or

$$-C_{L\delta_{a}}\delta_{a} \ge \beta C_{L_{g}} \tag{3.82}$$

where $C_{L\delta_a}$ is the rolling moment derivative due to elevon deflection obtained from aerodynamic module. As the elevon is employed as both elevator and aileron, the δ_a is the allowable angle for aileron function. In this study, $\delta_a \leq 0.5 \delta_{max}$. The elevon power required to give the specified roll performance concerns with dynamic movement of the aircraft with complex analysis; therefore, it will not be consider at this stage.

The outboard split-drag rudders are employed for the directional control for holding a zero sideslip angle. The size of rudder is determined base on the worse-case condition during landing and take-off in a crosswind ratio of 0.2 and sideslip angle of $\beta = 12^{\circ}$.

Considering the crosswind condition, at equilibrium

$$C_n = 0 = C_{n,o}\beta + C_{n,o}\delta_r \tag{3.83}$$

ОΓ

$$-C_{n\delta_{k}}\delta_{r} \ge C_{n_{\beta}}\beta \tag{3.84}$$

where $C_{n_{\beta}}$ is the change in the yawing moment coefficient of the aircraft due to sideslip angle, and $C_{n\delta_i}$ is the yawing moment coefficient due to the total split-drag rudder deflection δ_i including the upper and lower deflections.

For directional stability,

$$C_{n_g} > 0 ag{3.85}$$

By employing the equivalent wing, the empirical equation given in Raymer [22] is used to estimate C_{n_0} of a wing as

$$C_{n_{\beta}} = C_L^2 \left[\frac{1}{4\pi A} - \frac{\tan \Lambda_{1/2}}{\pi A(A + 4\cos \Lambda_{1/2})} \left(\cos \Lambda_{1/4} - \frac{A}{2} - \frac{A^2}{8\cos \Lambda_{1/2}} + 6 \frac{(x_{ac} - x_{CG})}{\overline{c}} \frac{\sin \Lambda_{1/2}}{A} \right) \right]$$
(3.86)

The $C_{n\delta_R}$ is the yawing moment coefficient due to the total split-drag rudder deflection δ_r about the aircraft center of gravity. The yawing moment due to drag of the split rudder is obtained from the aerodynamic module. In this study, the maximum half rudder deflection $(\delta_r/2)_{max} \le 20^\circ$.

4. Case Studies and Discussions

4.1 Requirements

In this study, the requirements for AU designs are specified as closely as those publicly available for Boeing X-45C. Likewise, the requirements for NU designs are specified as closely as those publicly available for Northrop X-47B. Some mission and all point performances, however, are assumed similarly to typical combat aircraft. The mission and point performance requirements for AU and NU designs are given in Table 4.1 and 4.2. The requirement at the design point in which the aircraft is to trim without elevon deflection is given in Table 4.3.

Table 4.1 Mission requirement of AU and NU designs

Phase	Code	Altitude	Mach	Data1	Data2	Data3
Warm-up & Taxi	1	0.0	0.0	1.0	0.0	0.0
Takeoff	2	0.0	0.0	0.03	1.1	0.0
Climb	3	12200.0	0.80	0.0	0.0	0.0
Cruise	4	12200.0	0.80	2400 km [AU]	0.0	0.0
				3250 km [NU]		
Loiter/C.A.P.	7	12200.0	0.50	15.0 min	0.0	0.0
Descend	3	6000.0	0.50	0.0	0.0	0.0
Weapon drop	6	6000.0	0.50	0.50 (F-Pay)	0.0	0.0
Climb	3	12200.0	0.80	0.0	0.0	0.0
Cruise	4	12200.0	0.80	2400 km [AU]	0.0	0.0
				3250 km [NU]		
Descend	3	0.0	0.3	0.0	0.0	0.0
Landing	8	0.0	0.0	0.0	0.0	0.0
End mission	0	0.0	0.0	0.06 (F-Fuel)	0.0	0.0

Table 4.2 Performance requirement of AU and NU designs

Phase	Code	Altitude	Mach	Data1	Data2 (F-Fuel)	Data3 (F-Payload)	Data4	Data5	Data6
Takeoff	1	0.0	0.0	0.0	0.95	1.0	0.0	0.0	≤750.0 m
Attained turn	2	6000.0	0.70	1.0	0.50	1.0	0.0	0.0	≥6.0 G
Sustained turn	3	6000.0	0.50	1.0	0.50	1.0	0.0	0.0	≥4.0 G
Sustained turn	3	12200.0	0.80	1.0	0.50	1.0	0.0	0.0	≥3.0 G
Landing	0	0.0	0.0	0.4	0.90	1.0	0.0	0.0	≤750.0 m

Table 4.3 Requirement at the design point of AU and NU designs

Altitude (m)	Mach	Fuel (F-Fuel)	Payload (F-Payload)
12200.0	0.80	0.5	1.0

4.2 Design Variables and Constraints

The formulation of MVO begins with identifying: a set of design variables X(I), the objective function to be minimized and constraint functions G(I) to be satisfied. There are 14 design variables and 37 constraints for AU design as listed in Table 4.4. For NU design, 15 design variables and 40 constraints are involved as shown in Table 4.5. The takeoff mass M_{to} is chosen as the objective function. The LSGRG2 optimizer then searches for the optimum solution -the minimum takeoff mass- that satisfies all constraints by altering the design variables. The values of design variables must not violate their specified bounds, and the values of constraints must not be negative, i.e. $G(I) \ge 0$. The constraint is said to be active or binding when G(I) = 0, namely, the optimum design is on the constraint bound. The moment about the center of gravity at the design point, the fuel tank volume required and the difference between mission fuel and fuel from fuel fraction are set as equality constraints to ensure practical and consistent designs; therefore, they are always binding. Examples of all input files containing design variables, parameters and constraints, are given in Appendix B.

Table 4.4a Design variables of AU design

X(I)	Design Variables			
1	Center chord (m)			
2	Tip chord (m)			
3	Semi-span (m)			
4	Kink chord (m)			
5	Kink station (y/b/2)			
6	LE sweep angle (deg)			
7	TED constant chord ratio			
8	Twist angle (deg)			
9	Thrust scale factor			
10	Fuel fraction			
11	CG height above ground			
12	Engine X-CG (fc)			
13	X-Main gear attachment (fc)			
14	Fuel tank outer panel (y/b/2)			

Note: fc = chordwise distance as fraction of local chord from leading edge y/b/2 = spanwise distance as fraction of semi-span from centerline

Table 4.4b Design constraints of AU design

G(I)	Design Constraints	G(I)	Design Constraints
1	Take-off mass [Objective Function]	20	Fuel tank volume required [=0]
2	Weapon bay & Nose gear bay	21	Mcg at design point [=0]
3	Rear spar & Weapon bay	22	Available angle to trim at landing
4	Intake & Front spar	23	Available angle at takeoff rotation
5	C/L TE & nozzle	24	Available angle to trim at attained turn
6	Static Margin at takeoff	25	Available angle to trim at sustained turn
7	Main gear & Front spar	26	Mission fuel - Fuel from fraction [=0]
8	Rear spar & Main gear	27	Mission Fuel: (thrust-drag)/thrust >0
9	Tipback angle at aft CG	28	Take-off ground distance
10	Tail down at wing tip	29	Attained turn Gs
11	Tail down at C/L	30	Sustained turn rate (Thrust>=Drag)
12	Max nose gear load (<15% MTO)	31	Sustained turn CL < CLtr, max
13	Max main gear load (<90% MTO)	32	Sustained turn rate (Thrust>=Drag)
14	C/L TE & Kink TE	33	Sustained turn CL < CLtr, max
15	Tip TE & Kink TE	34	Landing ground distance
16	Kink chord & Tip chord	35	Lateral stability [-dCL/dBeta >0]
17	Outer fuel tank & Inner station	36	Elevon (aileron): Cross-wind case
18	Max thickness available at C/L	37	Directional stability [dCN/dBeta >0]
19	Main gear bay & Kink station [=0]	38	Split-rudder sizing: Cross-wind case

Table 4.5a Design variables of NU design

X(I)	Design Variables			
1	Center chord (m)			
, 2	Tip chord (m)			
3	Semi-span (m)			
4	Kink chord (m)			
5	LE inner sweep angle (deg)			
6	LE outer sweep angle (deg)			
7.	TED constant chord ratio			
→ 8	Twist angle (deg)			
9	Thrust scale factor			
10	Fuel fraction ·			
†1	CG height above ground			
12	Engine X-CG (fc)			
13	X-Main gear attachment (fc)			
14	Fuel tank inner panel (y/b/2)			
15	Fuel tank outer panel (y/b/2)			

Note: fc = chordwise distance as fraction of local chord from leading edge y/b/2 = spanwise distance as fraction of semi-span from centerline

Table 4.5b Design constraints of NU design

G(I)	Design Constraints		
1	Take-off mass [Objective Function]	21	Kink station & Outer fuel tank
2	Weapon bay & Nose gear bay	22	Inner sweep & Outer sweep
3	Rear spar & Weapon bay	23	Mcg at design point [=0]
4	Intake & Front spar	24	Available angle to trim at landing
5	C/L TE & nozzle	25	Available angle at takeoff rotation
6	Static Margin at takeoff	26	Available angle to trim at attained turn
7	Main gear & Front spar	27	Available angle to trim at sustained turn
8	Rear spar & Main gear	28	Mission fuel - Fuel from fraction {=0}
9	Tipback angle at aft-CG	29	Mission Fuel: (thrust-drag)/thrust >0
10	Tail down at wing tip	30	Take-off ground distance
11	Tail down at C/L	31	Attained turn Gs
12	Max nose gear load (<15% MTO)	32	Sustained turn rate (Thrust>=Drag)
13	Max main gear load (<90% MTO)	33	Sustained turn CL < CLtr, max
14	C/L TE & Kink TE	34	Sustained turn rate (Thrust>=Drag
15	Tip TE & Kink TE	35	Sustained turn CL < CLtr,max
16	Kink chord & Tip chord	36	Landing ground distance
17	Outer fuel tank & Inner station	37	Lateral stability [-dCL/dBeta >0]
18	Max thickness available at C/L	38	Elevon (aileron): Cross-wind case
19	Inner fuel tank & Main gear bay {=0]	39	Directional stability [dCN/dBeta >0]
20	Fuel tank volume required [=0]	40	Split-rudder sizing: Cross-wind case

4.3 Case Studies

In this study, ten basic design cases with variation of minimum static margin ranging from 0 to -20 are investigated as shown in Table 4.6. Note that the kink station for the basic NU designs is fixed at a fraction of 0.4 of the wing semi-span.

Table 4.6 Design case studies

Design Cases	Minimum Static Margin (SM = $\%\overline{\overline{c}}$)
AUI & NUI	0
AU2 & NU2	-5
AU3 & NU3	-10
AU4 & NU4	-15
AU5 & NU5	-20

In addition, an AU-X case is investigated to study the effects of the NU requirements on the AU configuration; and two NU designs with the kink stations at fractions of 0.5 and 0.6 of semi-span are also studied, called NU-Ks cases. Symmetrical airfoils are used for all design case with NACA 66-018, 64A010 and 64A008 applied at the center, kink and tip stations, respectively.

4.4 Results and Discussions

The optimum values of the design variables and constraints for AU designs are as shown in Tables 4.7a and 4.7b; and those for NU designs are as shown in Tables 4.8a and 4.8b, respectively. The bounds of design variables were specified to provide the search limit for the optimum design, and several constraints were imposed to ensure the practical design.

As can be seen, all designs were driven by the static margin constraint at takeoff as seen from G(6). Relaxing stability (more negative static margin or unstable) resulted in smaller aircraft as indicated by X(1) to X(3), and lighter weight as shown by the objective function G(1) which lead to smaller engines and less fuel required as seen from X(9) and X(10), respectively. However, the benefit of 'mass reduction was decreased as the static margin was further relaxed as indicated by percentage reduction in takeoff mass G(1) for both AU and NU designs.

The leading-edge sweep angle, employed typically to avoid drag rise at high subsonic flight, was obtained with a very high value compared with typical subsonic aircraft as indicated by X(6) for AU and X(5) for NU designs. The high sweep reduces aerodynamic efficiency and increases structural weight. However, the highly swept, wing design was obtained mainly due to the requirement of a large moment arm for pitch stability and control. On the other hand, for NU designs, the outer wing sweep X(6) was kept smaller to provide better aerodynamic efficiency for low speed flight such as takeoff and landing.

It can be seen that all structural clearance constraints such as G(2) and G(3) were all binding (G(I) = 0) to keep minimum size and weight. All equality constraints are active as expected. For AU designs, the engines were sized mainly based on the thrust required for the attained turn requirement as seen from G(28), while the required thrusts for the climb and attained turn requirements were the key design parameters driven the engine size for NU designs as seen from G(29) and G(31). The wing area was determined by the landing requirement as seen from G(33) for AU designs and G(36) for NU designs. The nose landing gear was attached at a fixed fraction of center chord close to the wing apex and was sized to carry load not greater than 15% of the takeoff weight as seen from the binding constraint G(12).

It can be seen that there were sufficient control powers for the elevons to trim at landing, attained turn and sustained turn; and for rotation at takeoff as indicated by positive values of G(21) to G(24) for AU designs, and G(24) to G(27) for NU designs. All designs were laterally and directionally stable as seen from G(34) and G(36) for AU designs, and G(37) and G(39) for NU designs. There was sufficient elevon control power for lateral control, and split-rudder control power for directional control in crosswind flight as seen from G(35) and G(37) for AU designs and G(38) and G(40) for NU designs. Note that the elevons and split-rudders were not sized to their minimum dimensions. This is due to the constant fraction of chord and span of the elevons and split-rudders specified by the user. For AU designs, the elevons and split-rudders had equal span on the outer wing. For NU designs, the elevon was spanned over the inner wing, and the split-rudder was spanned over the outer wing.

Table 4.7a Design variables at the optimum AU designs

	Design Variables X(I)	Initial Values	Lower Bounds	Upper Bounds	AU1 sm >= 0%	AU2 sm >=-5%	AU3 sm >=-10%	AU4 sm >=-15%	AU5 sm >=-20%
1.	Center chord (m)	10.00	8.00	15.00	13.91	13.11	12.36	11.66	11.66
2.	Tip chord (m)	1.50	1.00	3.00	2.38	2.28	1.13	1.00	1.00
3.	Semi-span (m)	6.00	4.00	15.00	14.96	11.40	10.23	8.23	7.85
4.	Kink chord (m)	5.00	3.00	15.00	10.18	9.56	8.87	8.04	6.91
5.	Kink station (y/b/2)	0.30	0.10	0.60	0.17	0.18	0.19	0.24	0.25
6.	LE sweep angle (deg)	40.00	0.00	60.00	47.07	50.55	51.46	53.05	54.35
7.	TED constant chord ratio	0.30	0.25	0.30	0.25	0.25	0.25	0.25	0.25
8.	Twist angle (deg)	0.00	-5.00	5.00	-1.75	-1.41	-1.29	-0.12	0.89
9.	Thrust scale factor	1.00	0.80	2.00	1.73	1.33	1,13	1.18	1.12
10.	Fuel fraction	0.25	0.10	0.50	0.38	0.38	0.37	0.35	0.34
11.	CG height above ground	1.20	0.50	2.50	2.50	2.06	1.65	1.26	1.26
	Engine X-CG (fc)	0.50	0.40	0.80	0.72	0.72	0.70	0.66	0.68
	X-Main gear attachment (fc)	0.50	0.20	0.70	0.66	0.65	0.63	0.62	0.62
	Fuel tank outer panel (y/b/2)		0.10	0.95	0.25	0.27	0.29	0.37	0.42

Table 4.7b Design constraints at the optimum AU designs

Design Constraints	AU1 = sm >= 0% \(\overline{c}	AU2 = sm >=-5% C	AU3 sm>=-10% =	AU4 sm >=-15% C	AU5 = 5m >=-20% = 7
$[G(I) \ge 0]$	16541.33	13089.27	11015.24	9692.78	9048.43
. Take-off mass [Objective Function]	(0%)	(-20.87%)	(-33.41%)	(-41.40%)	(-45.30%)
. Weapon bay & Nose gear bay	0.000	0.000	0.000	0.000	0.000
. Rear spar & Weapon bay	0.000	0.000	0.000	0.000	0.00
Intake & Front spar	7.019	6.501	5.971	5.086	5.37
C/L TE & nozzle	1.295	1.452	1.540	1.827	1.58
Static Margin at takeoff	0.000	0.000	0.000	0.000	0.00
Main gear & Front spar	4.634	4.265	3.814	3.262	3.35
Rear spar & Main gear	0.705	0.775	0.871	1.007	0.42
Tipback angle at aft CG	0.208	0.249	0.286	0.321	0.32
Tail down at wing tip	0.000	0.000	0.000	0.000	0.00
I. Tail down at C/L	12.638	8.865	4.958	0.907	0.91
2. Mex nose gear load (<15% MTO)	0.000	0.000	0.000	0.000	0.00
3. Max main gear load (<90% MTO)	5.000	5.000	5.000	5.000	5.00
4. C/L TE & Kink TE	0.000	0.000	0.000	0,000	1.01
5. Tip TE & Kink TE	5.556	4.028	2.612	1.282	2.29
6. Kink chord & Tip chord	7.794	7.273	7.736	7.039	5.91
7. Outer fuel tank & Inner station	1.128	1.006	0.976	1.037	1.32
8. Max thickness available at C/L	0.294	0.293	0.235	0.090	0.11
9. Main gear bay & Kink station (=0)	0.000	0.000	0.000	0.000	0.00
Fuel tank volume required [=0]	0.000	0.000	0.000	0.000	0.00
l. Mcg at design point [=0]	0.000	0.000	0.000	0.000	0.00
2. Available angle to trim at landing	0.272	5,132	6.976	6.232	0.00
3. Available angle at takeoff rotation	0.272	5.132	6.976	6.232	00,00
4. Available angle to trim at attained turn	0.045	4.458	5.874	8.242	3.08
5. Available angle to trim at sustained turn	0.045	4.458	5.874	8.242	3.08

Table 4.7b (continued)

Design Constraints $[G(I) \ge 0]$	AU1 sm >= 0% ¯	AU2 sm >=-5% C	AU3 sm >=-10% \overline{C}	AU4 sm >=-15% $\overline{\overline{C}}$	AU5 sm >=-20% =
26. Mission fuel - Fuel from fraction [=0]	0.000	0.000	0.000	0.000	0.000
27. Mission Fuel: (thrust-drag)/thrust >0	0.000	0.000	0.037	0.156	0.192
28. Take-off ground distance	0.222	0.202	0.212	0.309	0.362
29. Attained turn Gs	0.000	0.000	0.000	0.000	0.000
30. Sustained turn rate (Thrust>=Drag)	0.314	0.148	0.138	0.095	0.085
31. Sustained turn CL < CLtr,max	0.230	0.239	0.246	0.272	0.344
32. Sustained turn rate (Thrust>=Drag)	0.155	0.000	0.000	0.000	0.000
33. Sustained turn CL < CLtr,max	0.307	0.323	0.336	0.377	0.457
34. Landing ground distance	0,000	0.000	0.000	0.000	0.083
35. Lateral stability [-dCL/dBeta >0]	0.0137	0.0187	0.0180	0.0230	0.0280
36. Elevon (aileron): Cross-wind case	0.0231	0.0186	0.0189.	0.0155	0.0148
37. Directional stability [dCN/dBeta >0]	0.0003	0.0004	0.0005	0.0007	0.0010
38. Split-rudder sizing: Cross-wind case	0.0012	0.0011	0.0009	0.0008	0!0007

Table 4.8a Design variables at the optimum NU designs

	Design Variables X(I)	Initial Values	Lower Bounds	Upper Bounds	NU1 sm >= 0%	NU2 sm >=-5%	NU3 sm >=-10%	NU4 sm >=-15%	NU5 sm >=-20%
1.	Center chord (m)	10.00	8.00	15.00	13.22	13.22	13.22	13.22	13.22
2.	Tip chord (m)	1.50	1.00	5.00	4.70	4.20	3.26	2.61	2.09
3.	Semi-span (m)	6.00	4.00	15.00	14.11	11.71	11.21	10.90	10.66
4.	Kink chord (m)	6.00	2.00	15.00	5.03	4.20	3.26	2.61	2.09
5.	LE inner sweep angle (deg)	40.00	0.00	60.00	51.86	55.51	56.38	57.17	60.00
6.	LE outer sweep angle (deg)	30.00	0.00	60.00	8.91	17.37	25.55	30.47	19.98
7.	TED constant chord ratio	0.30	0.25	0.30	0.25	0.25	0.25	0.25	0.25
8.	Twist angle (deg)	0.00	-5.00	5.00	-2.46	-1.67	-1.33	-1.15	-1.51
9.	Thrust scale factor	1.00	0.60	2.00	1.25	1.00	0.86	0.77	0.71
10.	Fuel fraction	0.25	0.10	0.50	0.39	0.38	0.37	0.36	0.35
11.	CG height above ground	1.20	0.50	2.50	1.46	1.46	1.46	1.46	1.46
12.	Engine X-CG (fc)	0.50	0.40	0.80	0.48	0.53	0.58	0.60	0.61
13.	X-Main gear attachment (fc)	0.50	0.20	0.70	0.59	0.59	0.59	0.59	0.59
14.	Fuel tank inner panel (y/b/2)	0.30	0.10	0.95	0.14	0.17	0.18	0.18	0.19
	Fuel tank outer panel (y/b/2)	0.50	0.10	0.95	0.22	0.26	0.28	0.29	0.29

Table 4.8b Design constraints at the optimum AU designs

	Design Constraints	NUI	NU2	NU3	NU4	NU5
	$[G(I) \geq 0]$	$sm >= 0\% \overline{\overline{C}}$	$sm >=-5\% \overline{\overline{C}}$	sm >=-10 % \overline{\overline{C}}	sm >=-15% $\overline{\overline{C}}$	sm >=-20% =
1.	Take-off mass [Objective Function]	16533.68 (0%)	13545.25 (-18.07%)	<u>11960.44</u> (-27.66%)	<u>10971.12</u> (-33.64%)	<u>10215.80</u> (-38.21%)
2.	Weapon bay & Nose gear bay	0.000	0.000	0.000	0.000	0.000
3.	Rear spar & Weapon bay	0.000	0.000	0.000	0.000	0.000
4.	Intake & Front spar	2.296	3.118	3.714	4.097	4.210
5.	C/L TE & nozzle	2.821	2.480	2.167	1.978	2.023
6.	Static Margin at takeoff	0.000	0.000	0.000	0.000	0.000
7.	Main gear & Front spar	3.457	3.309	3.327	3.321	3.072
8.	Rear spar & Main gear	1.919	1.665	1.394	1.221	1.318
9.	Tipback angle at aft-CG	0.303	0.303	0.303	0.303	0.303
10.	Tail down at wing tip	0.000	0.000	0.003	0.000	4.933
11,	Tail down at C/L	0.000	0.000	0.000	0.000	0.000
12.	Max nose gear load (<15% MTO)	0.000	0.000	0.000	0.000	0.000
13.	Max main gear load (<90% MTO)	5.000	5.000	5.000	5.000	5.000
14.	C/L TE & Kink TE	0.000	1.198	2.217	2.849	2.747
15.	Tip TE & Kink TE	1.000	2.198	3.216	3.849	2.325
16.	Kink chord & Tip chord	0.328	0.000	0.000	0.000	0.000
17.	Outer fuel tank & Inner station	1.042	1.075	1.097	1.124	1.158
18.	Max thickness available at C/L	0.006	0.150	0.233	0.290	0.335
19.	Inner fuel tank & Main gear bay [=0]	0.000	0.000	0.000	0.000	0.000
20.	Fuel tank volume required [=0]	0.000	0.000	0.000	0.000	0.000
21.	Kink station & Outer fuel tank	2.562	1.597	1.390	1.251	1.127
22.	Inner sweep & Outer sweep	42.943	38.139	30.825	26.700	40.018
23.	Mcg at design point [=0]	0.000	0.000	0.000	0.000	0.000
24.	Available angle to trim at landing	0.178	3.834	4.770	5.905	5.842
25.	Available angle at takeoff rotation	0.178	3.834	4.770	5.905	5.842
26.	Available angle to trim at attained turn	0.000	3.072	3.319	3.829	3.393
27.	Available angle to trim at sustained turn	0.000	3.072	3.319	3.829	3.393
28.	Mission fuel - Fuel from fraction [=0]	0.000	0.000	0.000	0.000	0.000
29.	Mission Fuel: (thrust-drag)/thrust >0	0.000	0.000	0.000	0.000	0.000
30.	Take-off ground distance	0.200	0.179	0.164	0.150	0.137
31.	Attained turn Gs	0.000	0.000	0.000	0.000	0.000
32.	Sustained turn rate (Thrust>=Drag)	0.275	0.157	0.154	0.151	0.149
33.	Sustained turn CL < CLtr,max	0.288	0.295	0.299	0.299	0.310
34.	Sustained turn rate (Thrust>=Drag)	0.110	0.000	0.000	0.000	0.000
35.	Sustained turn CL < CLtr, max	0.377	0.392	0.401	0.407	0.424
36.	Landing ground distance	0.000	0.000	0.000	0.000	0.000
37.	Lateral stability [-dCL/dBeta >0]	0.0169	0.0238	0.0252	0.0263	0.0258
38.	Elevon (aileron): Cross-wind case	0.0106	0.0081	0.0085	0.0088	0.0095
39.	Directional stability [dCN/dBeta >0]	0.0004	0.0005	0.0007	0.0008	0.0009
40.	Split-rudder sizing: Cross-wind case	0.0021	0.0019	0.0017	0.0015	0.0013

The total mass and component mass were listed in Table 4.9 for AU designs and Table 4.10 for NU designs. It can be seen that relaxing static margin has more impact on the takeoff mass of AU designs than NU designs. The wing geometry and mass breakdown are given in Tables 4.11 and 4.12 for AU and NU designs, respectively. The wing mass was estimated based on aluminium material. A factor of 0.8 was applied to the wing mass to account for the composite wing design employed in this study as suggested in Raymer [22]. The equivalent wing planform was used for aerodynamic drag and stability evaluations.

The component center of gravity (CG) and the excursion of center of gravity were calculated and given in Tables 4.13 and 4.14. As the aircraft CG location has significant impact on the required static margin, the payload CG and fuel CG were enforced to locate at the operating empty mass CG to avoid CG movement during flight. Therefore, the forward and aft CG limits are identical. A number of internal packaging constraints were imposed to ensure CG consistency. The dimensions of landing gear bay and engine bay were calculated and given in Tables 4.15 and 4.16. These were used as design constraints for internal packaging to ensure practical design. An example of mission fuel estimation is given in Table 4.17 for AU3 design.

An additional AU design called AU-X was investigated with the same requirement as the NU3 design. The optimum design of the AU-X is given in Table 4.18. It can be seen that the AU-X design had much larger weight than the NU3 design. This indicated that the single leading-edge cranked planform of NU was more (aerodynamically) efficient than the straight leading-edge planform of AU for longer range or larger aircraft.

Further NU design cases with variation of kink stations called NU-Ks were investigated and the optimum designs are as shown in Table 4.19. It can be seen that the shorter the kink station, the smaller (and lighter) the aircraft. The shorter kink station indicates the longer outer-wing span and larger area. With the larger wing area of the outer wing associated with smaller sweep compared with the inner-wing sweep, the wing planform is more aerodynamically and structurally efficient; and more adaptable to achieve stability requirement leading to lighter and smaller design.

Table 4.9 Mass breakdown of the optimum AU designs

M D 11 (1)	AU1	AU2	AU3	AU4	AU5
Mass Breakdown (kg)	$sm >= 0\% \overline{\overline{C}}$	sm >≃-5% ¯	sm >=-10% $\overline{\overline{c}}$	sm>=-15% ¯	sm >=-20% $\overline{\widetilde{C}}$
Engine + Fuel system	2111.43	1578.48	1328.67	1387.78	1311.63
Payload	2040.00	2040.00	2040.00	2040.00	2040.00
Communication + Data system	80.00	80.00	80.00	80.00	80.00
Hydraulics + Flying control	330.83	261.79	220.30	193.86	180.97
Avionics + Instruments + Electrics	496.24	392.68	330.46	290.78	271.45
Air condition + De-icing	165.41	130.89	110.15	96.93	90.48
Furnishing	165.41	130.89	110.15	96.93	90.48
Landing gear	1788.18	1426.11	1132.86	883.19	868.11
Fuel mass	6361.26	4939.75	4035.13	3375.39	3038.57
Wing structure	3002.56	2108.68	1627.52	1247.93	1076.74
Takeoff mass, Mto	16541.33	13089.27	11015.24	9692.78	9048.43
Zero fuel mass, Mzf	10180.07	8149.52	6980.11	6317.39	6009.86
Zero payload, Mzp	14501.33	11049.27	8975.24	7652.78	7008.43
Operating empty mass, OEM	8140.07	6109.52	4940.11	4277.39	3969.86

Table 4.10 Mass breakdown of the optimum NU designs

	NU1	NU2	NU3	NU4	NU5
Mass Breakdown (kg)	sm >= 0% ¯	sm >=-5% $\overline{\overline{C}}$	sm >=-10% $\overline{\overline{C}}$	sm >=-15% ¯	sm >=-20 % ¯
Engine + Fuel system	2566.85	1992.37	1695.58	1510.15	1368.64
Payload	2040.00	2040.00	2040.00	2040.00	2040.00
Communication + Data system	80.00	80.00	80.00	80.00	80.00
Hydraulics + Flying control	330.67	270.91	239.21	219.42	204.32
Avionics + Instruments + Electrics	496.01	406.36	358.81	329.13	306.47
Air condition + De-icing	165.34	135.45	119.60	109.71	102.16
Furnishing	165.34	135.45	119.60	109.71	102.16
Landing gear	1136.77	1080.64	1047.03	1024.32	1005.93
Fuel mass	6523.88	5204.75	4446.57	3963.45	3589.30
Wing structure	3028.82	2199.31	1814.04	1585.22	1416.82
Takeoff mass, Mto	16533.68	13545.25	11960.44	10971.12	10215.80
Zero fuel mass, Mzf	10009.80	8340.50	7513.87	7007.67	6626.50
Zero payload, Mzp	14493.68	11505.25	9920.44	8931.12	8175.80
Operating empty mass, OEM	7969.80	6300.50	5473.87	4967.67	4586.50

Table 4.11 Wing geometry and mass of the optimum AU designs

Wing Geometry	AU1	AU2	AU3	AU4	AU5
Wing span (m)	29.92	22.79	20.46	16.46	15.70
Kink span (m)	5.08	4.19	3.97	3.94	3.93
LE Sweep (deg)	18.82	20.26	20.60	22.34	10.46
1/2 Sweep (deg)	18.82	20.26	20.60	22.34	10.46
t/c center-line	0.18	0.18	0.18	0.18	0.18
t/c kink	01.0	0.10	0.10	0.10	0.10
t/c tip	0.08	0.08	0.08	0.08	0.08
Center-line chord (m)	13.91	13.11	12.36	11.66	11.66
Kink chord (m)	10.18	9.56	8.87	8.04	6.91
fip chord (m)	2.38	2.28	1.13	1.00	1.00
Wing area, inner (m²)	61.22	47.51	42.16	38.83	36.46
Wing area, outer (m2)	155.96	110.13	82.40	56.58	46.56
Wing area, total (m²)	217.18	157.64	124.56	95.40	83.02
Outer wing area ratio	0.72	0.70	0.66	0.59	0.56
.ED area (m²)	0.00	0.00	0.00	0.00	0.00
Elevon area (m²)	25.54	17.99	14.29	9.83	7.99
Split-rudder planform area (m²)	13.45	9.54	6.31	4.32	3.65
Max Tensile stress (MPa)	350.00	350.00	350.00	350.00	350.00
Max Comp stress (MPa)	253.85	239.42	229.32	222.10	218.32
Rho*g, Al (kN/m³)	28.00	28.00	28.00	28.00	28.00
Material for bending (N)	5666.43	2921.99	2016.16	1265.11	968.94
Material for shear (N)	2868.98	1840.11	1449.02	1055.05	895.65
Fuel relief factor at Kink	0.17	0.17	0.16	0.16	0.15
Fuel relief factor at Center-line	0.29	0.29	0.29	0.31	0.30
Structure relief factor at Kink	0.09	0.09	0.08	0.07	0.07
Structure relief factor at Center-line	0.12	0.12	0.12	0.12	0.11
Total relief at Kink	0.74	0.74	0.75	0.77	0.78
Total relief at Center-line	0.57	0.56	0.57	0.56	0.56
Rib weight (N)	17980.73	12829.31	9838.55	7561.87	6433.17
deal box weight, inner (N)	9764.14	6970.12	5877.30	5084.58	4583.13
deal box weight, outer (N)	13828.65	8972.50	6235.11	3960.70	3051.72
deal box weight, total (N)	23592.79	15942.62	2112.41	9045.28	7634.85
Total penalty weight (N)	2746.68	2269.02	1993.41	1832.02	1710.15
Fixed LED&TED weight (N)	3244.30	2567.24	2160.45	1901.07	1774.70
LED weight (N)	0.00	0.00	0.00	0.00	0.00
Elevon weight (N)	3762.78	2627.66	2073.51	1420.01	1152.61
Split-rudder weight (N)	3459.75	2442.29	1610.87	1099.14	926.66
Total wing mass (kg)	3002.56	2108.68	1627.52	1247.93	1076.74

Table 4.11 (continued)

Wing Geometry	AU1	AU2	AU3	AU4	AU5
Equivalent Wing Planform:					
Tip chord	2.38	2.28	1.13	1.00	1.00
Root chord	12.14	11.55	11.05	10.59	9.58
Taper ratio	0.20	0.20	0.10	0.09	0.10
Geometric mean chord	7.26	6.92	6.09	5.80	5.29
Aerodynamic mean chord, $\overline{\overline{c}}$	8.35	7.95	7.43	7.12	6.45
Aspect ratio	4.12	3.30	3.36	2.84	2.97
Wing area	217.18	157.64	124.56	95.40	83.01
LE sweep (deg)	47.07	50.55	51.46	53.05	54.35
1/4 sweep (deg)	42.37	45.34	45.37	46.07	48.27
1/2 sweep (deg)	36.84	38.97	37.62	36.75	40.29

Table 4.12 Wing geometry and mass of the optimum NU designs

Wing Geometry	NU1	NU2	NU3	NU4	NU5
Wing span (m)	28.23	23.42	22.42	21.80	21.31
Kink span (m)	11.29	9.37	8.97	8.72	8.52
Fixed kink station (y/b/2)	0.40	0.40	0.40	0.40	0.40
LE Sweep, inner (deg)	51.86	55.51	56.38	57.17	60.00
LE Sweep, outer (Deg)	8.91	17.37	25.55	30.47	19.98
1/2 Sweep, inner (deg)	28.73	26.25	21.47	18.46	23.10
1/2 Sweep, outer (deg)	7.83	17.37	25.55	30.47	19.98
t/c center-line	0.18	0.18	0.18	0.18	0.18
t/c kink	0.10	0.10	0.10	0.10	0.10
t/c _a tip	0.08	0.08	0.08	80.0	0.08
Center-line chord (m)	13.22	13.22	13.22	13.22	13.22
Kink chord (m)	5.03	4.20	3.26	2.61	2.09
Tip chord (m)	4.70	4.20	3.26	2.61	2.09
Wing area, inner (m²)	103.03	81.62	73.88	69.03	65.25
Wing area, outer (m ²)	82.42	59.08	43.84	34.16	26.71
Wing area, total (m ²)	185.44	140.69	117.72	103.19	91.96
Outer wing area ratio	0.44	0.42	0.37	0.33	0.29
LED area (m²)	0.00	0.00	0.00	0.00	0.00
Elevon area (m²)	17.65	13.28	11.89	11.04	10.39
Split-rudder planform area (m²)	20.60	14.77	10.96	8.54	6.68
Max Tensile stress (MPa)	350.00	350.00	350.00	350.00	350.00
Max Comp stress (MPa)	253.82	241.48	234.09	229.09	225.04
Rho*g, Al (kN/m³)	28.00	28.00	28.00	28.00	28.00
Material for bending (N)	7290.20	4106.70	3123.43	2612.50	2306.98
Material for shear (N)	2668.09	1885.27	1614.22	1463.89	1364.59
Fuel relief factor at Kink	0.00	0.00	0.00	0.00	0.00
Fuel relief factor at Center-line	0.18	0.17	0.17	0.16	0.16
Structure relief factor at Kink	0.06	0.05	0.05	0.04	0.04

Table 4.12 (continued)

Wing Geometry	NU1	NU2	NU3	NU4	NU5
Structure relief factor at Center-line	0.12	0.12	0.11	0.10	0.10
Total relief factor at Kink	0.94	0.95	0.95	0.96	0.96
Total relief factor at Center-line	0.69	0.70	0.71	0.72	0.73
Rib weight (N)	15872.06	11803.34	9707.01	8463.85	7558.00
Ideal box weight, inner (N)	16789.43	12030.18	10315.19	9328.79	8753.83
Ideal box weight, outer (N)	6347.09	4214.10	2983.50	2280.46	1645.57
Ideal box weight, total (N)	23136.52	16244.28	13298.69	11609.25	10399.40
Total penalty weight (N)	2848.16	2333.36	2060.35	1889.93	1759.81
Fixed LED&TED weight (N)	3242.80	2656.67	2345.84	2151.80	2003.65
LED weight (N)	0.00	0.00	0.00	0.00	0.00
Elevon weight (N)	2599.19	1941.48	1731.32 '	1602.50	1503.53
Split-rudder weight (N)	5301.51	3784.06	2800.8	2178.64	1701.39
Total wing mass (kg)	3028.82	2199.31	1814.04	1585.22	1416.82
Equivalent Wing Planform:					
Tip chord	4.70	4.20	3.26	2.61	2.09
Root chord	8.44	7.81	7.24	6.85	6.54
Taper ratio	0.56	0.54	0.45	0.38	0.32
Geometric mean chord	6.57	6.01	5.25	4.73	4.31
Aerodynamic mean chord, $\overline{\overline{c}}$	6.75	6.19	5.50	5.05	4.70
Aspect ratio	4.30	3.90	4.27	4.61	4.94
Wing area	185,44	140.69	117.72	103.18	91.96
LE sweep (deg)	41.07	46.23	48.61	50.28	51.10
1/4 sweep (deg)	38.84	44.04	46.28	47.89	48.62
1/2 sweep (deg)	36.47	41.67	43.74	45.26	45.86

Table 4.13 Component of gravity locations of the optimum AU designs

Aircraft CG from Wing Apex (m)	AU1	AU2	AU3	AU4	AU5
Nose gear	4.53	4.15	3.80	3.46	3.46
Main gear	7.88	7.42	7.00	6.60	6.60
Avionics, Instruments, Electrics	3.78	3.62	3.47	3.33	3.33
Communication, Data system	3.78	3.62	3.47	3.33	3.33
Flying control, Hydraulic system	12.51	11.36	10.28	9.34	8.91
Air condition system	3.78	3.62	3.47	3.33	3.33
Furnishing	3.78	3.62	3.47	3.33	3.33
Engine	10.05	9.37	8.69	7.67	7.96
Weapon bay	8.26	7.65	7.09	6.57	6.57
Fuel tank	8.26	7.65	7.09	6.57	6.57
Wing structure	8.26	7.66	7.04	6.59	6.33
Wing structure $(\%\overline{\overline{c}})$	25.08	29.35	32.31	37.28	37.01
Operating empty mass, OEM	8.26	7.65	7.09	6.57	6.57
Zero fuel mass, MZF	8.26	7.65	7.09	6.57	6.57
Zero payload mass, MZP	8.26	7.65	7.09	6.57	6.57
Takeoff mass, MTO	8.26	7.65	7.09	6.57	6.57
Design Point CG	8.26	7.65	7.09	6.57	6.57
Aft CG	8.26	7.65	7.09	6.57	6.57
Forward CG	8.26	7.65	7.09	6.57	6.57
Static Margin at Design Point (% $\overline{\overline{c}}$)	0.00	-0.05	-0.10	-0.15	-0.20
Static Margin at MTO (% $\overline{\overline{c}}$)	0.00	-0.05	-0.10	-0.15	-0.20

Table 4.14 Center of gravity locations of the optimum NU designs

Aircraft CG from Wing Apex (m)	NU1	NU2	NU3	NU4	NU5
Nose gear	3.87	3.87	3.87	3.87	3.87
Main gear	7.04	7.04	7.04	7.04	7.04
Avionics, Instruments, Electrics	3.64	3.64	3.64	3.64	3.64
Communication, Data system	3.64	3.64	3.64	3.64	3.64
Flying control, Hydraulic system	10.86	10.41	10.06	9.84	9.71
Air condition system	3.64	3.64	3.64	3.64	3.64
Furnishing	3.64	3.64	3.64	3.64	3.64
Engine	6.35	7.07	7.61	7.95	8.03
Weapon bay	7.08	7.08	7.08	7.08	7.08
Fuel tank	7.08	7.08	7.08	7.08	7.08
Wing structure	8.45	8.03	7.67	7.45	7.40
Wing structure (% $\overline{\overline{c}}$)	43.07	42.20	40.98	40.57	42.75
Operating empty mass, OEM	7.08	7.08	7.08	7.08	7.08
Zero fuel mass, MZF	7.08	7.08	7.08	7.08	7.08
Zero payload mass, MZP	7.08	7.08	7.08	7.08	7.08
Takeoff mass, MTO	7.08	7.08	7.08	7.08	7.08
Design Point CG	7.08	7.08	7.08	7.08	7.08
Aft CG	7.08	7.08	7.08	7.08	7.08
Forward CG	7.08	7.08	7.08	7.08	7.08
Static Margin at Design Point (% $\overline{\overline{c}}$)	0.00	-5.00	-10.00	-15.00	-20.00
Static Margin at MTO (% $\overline{\overline{c}}$)	0.00	-5.00	-10.00	-15.00	-20.00

Table 4.15 Component sizing of the optimum AU designs

	AU1	AU2	AU3	AU4	AU5
Weapon Bay (2 JDAMs GBU-31)					
Payload mass (kg)	2040	2040	2040	2040	2040
Bay length (m)	3.75	3.75	3.75	3.75	3.75
Bay depth (m)	0.75	0.75	0.75	0.75	0.75
Bay width (m)	1.4	1.4	1.4	1.4	1.4
Landing Gear Design					
X-Nose gear attachment	3.28	3.12	2.97	2.83	2.83
Static load (%MTO)	15.00	15.00	15.00	15.00	15.00
Tyre diameter (m)	0.50	0.45	0.42	0.39	0.38
Tyre width (m)	0.16	0.14	0.13	0.12	0.12
Bay length (m)	2.90	2.46	2.05	1.66	1.66
Bay depth (m)	0.65	0.58	0.54	0.51	0.50
Bay width (m)	0.47	0.42	0.39	0.37	0.36
X-Main gear attachment	9.13	8.45	7.82	7.23	7.23
Y-Main gear attachment	2.20	1.79	1.70	1.70	1.70
Static load (%MTO)	85.00	85.00	85.00	85.00	85.00
Tyre diameter (m)	0.78	0.71	0.65	0.62	0.60
Tyre width (m)	0.24	0.22	0.20	0.19	0.19
Bay length (m)	3.30	2.86	2.45	2.06	2.06
Bay depth (m)	0.98	0.88	0.82	0.77	0.75
Bay width (m)	0.68	0.62	0.57	0.54	0.53
· Engine Sizing					
Thrust scale factor	1.73	1.33	1.13	F.18	1.12
Engine diameter (m)	1.16	1.02	0.94	0.96	0.93
length (m)	2.81	2.53	2.38	2.42	2.37
Uninstalled mass (kg)	1508.17	1127.49	949.05	991.27	936.88
Installed mass (kg)	2111.43	1578.48	1328.67	1387.78	1311.63
Thrust takeoff (kN)	84.58	64.93	55.51	57.7 5	54.87

Table 4.16 Component sizing of the optimum NU designs

	NU1	NU2	NU3	NU4	NU5
Weapon Bay (2 JDAMs GBU-31)					
Payload mass (kg)	2040	2040	2040	2040	2040
Bay length (m)	3.75	3.75	3.75	3.75	3.75
Bay depth (m)	0.75	0.75	0.75	0.75	0.75
Bay width (m)	1.4	1.4	1.4	1.4	1.4
Landing Gear Design					
X-Nose gear attachment	3.14	3.14	3.14	3.14	3.14
Static load (%MTO)	15.00	15.00	15.00	15.00	15.00
Tyre diameter (m)	0.50	0.46	0.43	0.42	0.40
Tyre width (m)	0.16	0.14	0.14	0.13	0.13
Bay length (m)	1.86	1.86	1.86	1.86	1.86
Bay depth (m)	0.65	0.59	0.56	0.54	0.53
Bay width (m)	0.47	0.43	0.41	0.39	0.38
X-Main gear attachment	7.77	7.77	7.77	7.77	7.77
Y-Main gear attachment	1.70	1.70	1.70	1.70	1.70
Static load (%MTO)	85.00	85.00	85.00	85.00	85.00
Tyre diameter (m)	0.78	0.72	0.68	0.65	0.63
Tyre width (m)	0.24	0.22	0.21	0.20	0.20
Bay length (m)	2.26	2.26	2.26	2.26	2.26
Bay depth (m)	0.98	0.90	0.85	0.82	0.79
Bay width (m)	0.68	0.63	0.59	0.57	0.55
Engine Sizing					
Thrust scale factor	1.25	1.00	0.86	0.77	0.71
Engine diameter (m)	1.32	1.18	1.10	1.04	0.99
length (m)	5.46	4.98	4.69	4.50	4.34
Uninstalled mass (kg)	1833.46	1423.12	1211.13	1078.68	977.60
Installed mass (kg)	2566.85	1992.37	1695.58	1510.15	1368.64
Thrust takeoff (kN)	81.80	64.97	56.11	50.50	46.18

Table 4.17 Mission fuel of the AU3 design

Mission Phase		Total Time	Total Mass	Fuel Consumption	Fuel Fraction	Total
		(min)	(kg)	at each phase (kg)	at each phase	Distance (km)
1.	Warm-up & Taxi	1.00	10946.01	69.24	0.9937	0.00
2.	Takeoff	1.26	10928.09	17.92	0.9984	0.00
3.	Clime	13.92	10603.86	324.23	0.9703	0.00
4.	Cruise	183.37	8962.40	1641.45	0.8452	2400.00
5.	Loiter/C.A.P.	198.37	8871.40	91.00	0.9898	2400.00
6.	Descend	199.05	8869.02	2.39	0.9997	2400.00
7.	Weapon drop	199.15	7849.02	0.0000	0.0000	2400.00
8.	Climb	208.23	7743.45	105.57	0.9866	2400.00
9.	Cruise	377.68	6227.72	1515.73	0.8043	4800.00
10.	Descend	379.82	6219.61	8.11	0.9987	4800.00
11.	Landing	383.55	6188.52	31.10	0.9950	4800.00
12.	End mission	383.55	6188.52	0.00	0.0000	4800.00

Table 4.18 The optimum AU-X design

Design Variables	AU-X
1. Center chord (m)	12.35
2. Tip chord (m)	1.00
3. Semi-span (m)	11.44
4. Kink chord (m)	9.07
5. Kink station (y/b/2)	0.18
6. LE sweep angle (deg)	48.51
TED constant chord ratio	0.25
8. Twist angle (deg)	-1.21
Thrust scale factor	0.98
10. Fuel fraction	0.39
 CG height above ground 	1.64
12. Engine X-CG (fc)	0.68
13. X-Main gear attachment (fc)	0.63
14. Fuel tank outer panel (y/b/2)	0.28
Performance requirement	As in NU design
Reference engine	P&W: F100-PW-220E
Static Margin at MTO (% $\overline{\overline{c}}$)	10.0
Takeoff mass (kg)	13163.89

Table 4.19 The optimum NU-Ks designs

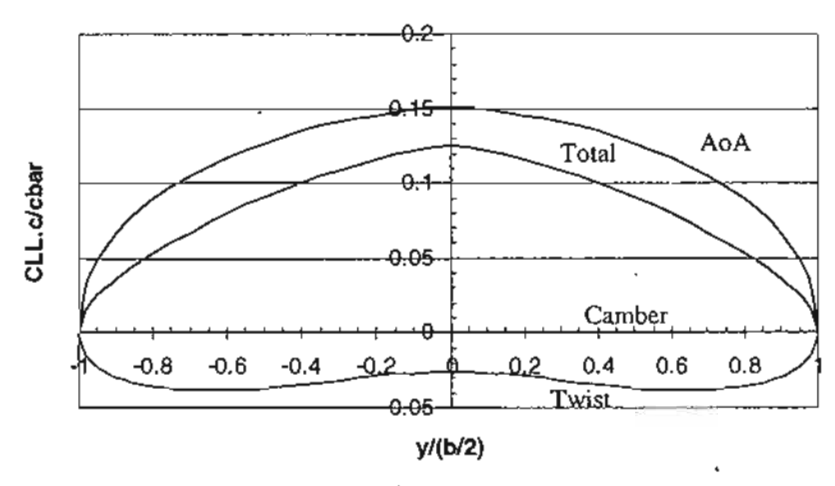
Design Variables	NU (sm >=-10% $\overline{\overline{c}}$)		
	Ks = 0.4	Ks = 0.5	Ks = 0.6
1. Center chord (m)	13.22	13.22	13.22
2. Tip chord (m)	3.26	3.02	2.63
3. Semi-span (m)	11.21	11.38	11.48
4. Kink chord (m)	3.26	3.02	2.63
5. LE inner sweep angle (deg)	56.38	53.51	52.24
6. LE outer sweep angle (deg)	25.55	23.76	10.00
7. TED constant chord ratio	0.25	0.25	0.25
8. Twist angle (deg)	-1.33	-1.60	-1.97
Thrust scale factor	0.86	0.91	0.95
Fuel fraction	0.37	0.38	0.38
CG height above ground	1.46	1.46	1.46
12. Engine X-CG (fc)	0.58	0.55	0.52
13. X-Main gear attachment (fc)	0.59	0.59	0.59
14. Fuel tank inner panel (y/b/2)	0.18	0.18	0.17
15. Fuel tank outer panel (y/b/2)	0.28	0.25	0.24
Takeoff mass (kg)	11960.44	12547.69	12960.14

Note Ks = the kink station as the fraction of semi-span wing from the centerline

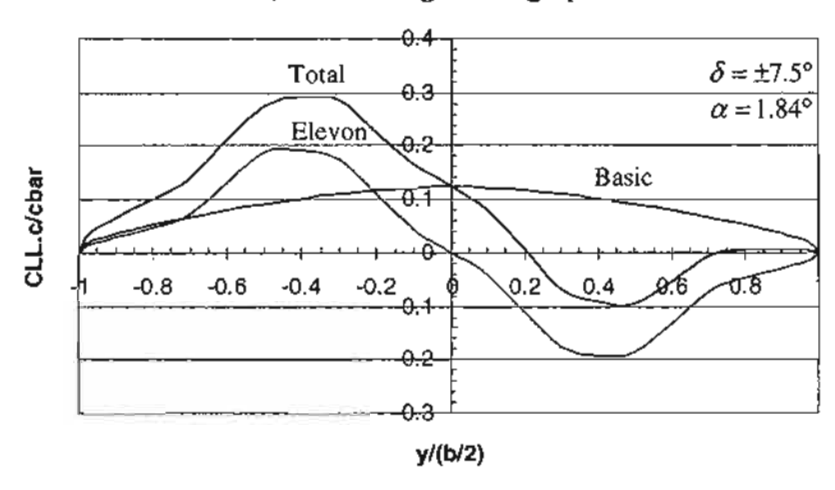
The aerodynamic loads of AU3 and NU3 designs are as shown Figs. 4.1 and 4.2, respectively. It can be seen from Figs. 4.1a and 4.2a that the total lift coefficient of the basic wing (i.e. wing without control deflection) at the design point is the sum of lift coefficients due to the wing camber, twist and angle of attack of a given planform. Note that there is a slightly bumpy rise at the outboard section of the NU3 basic wing as shown in Fig. 4.2a. This is mainly due to the smaller sweep at the outboard wing providing an increase in lift coefficient. The contributions of elevons functioning as ailerons are as shown in Figs. 4.1b and 4.2b. As can be seen, the lift contribution of elevons had major influence at the inboard section where they were located resulting in a positive lift on the port, and negative lift on the starboard wing causing roll. The contributions of elevons functioning as elevators at takeoff are given as shown in Figs. 4.1c and 4.2c. Note that the total lift coefficients for each flight condition are used to obtain control derivatives for stability and control estimations.

For a stealthy design, the sharp leading edge of the wing is preferred to the rounded leading edge to reduce the radar cross section (see Boeing X-45C and Northrop X-47B). The combination of sharp leading edge and high swept planform can produce the leading-edge vortices that enhance the lift at high angle of attack, and increase the stall angle as explained in Anderson [29]. However, due to the complex aerodynamic characteristics and lack of reliable estimation, the leading-edge vortices are not considered. In this study, the stall angle with control deflection was assumed conservatively to be 12° and the aerodynamic lift and drag were estimated on the basis of typical rounded leading-edge wing.

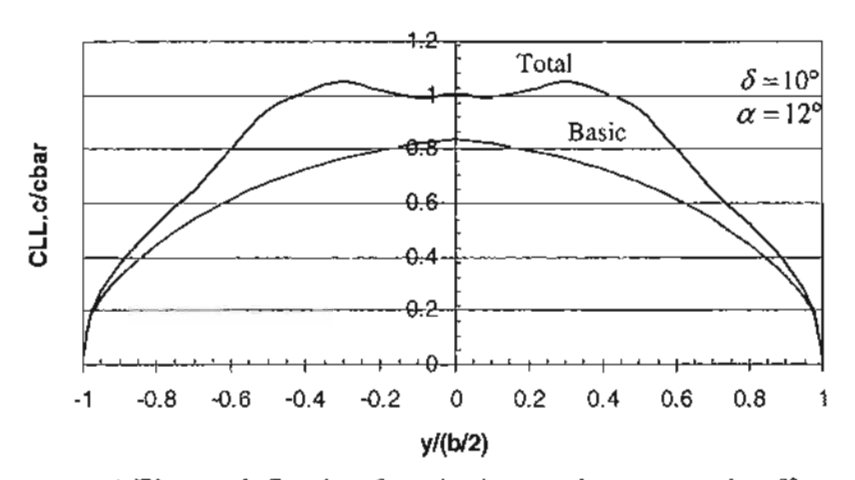
The convergence histories of takeoff mass (the objective function) and static margin constraint $(G(6) \ge 0)$ of the AU3 design are illustrated in Figs. 4.3 and 4.4, respectively. It can be seen that 46 iterations driven by the LSGRG2 optimizer were required to achieve the optimum design, i.e. minimized takeoff mass. It also shows a strong influence of the static margin on the takeoff mass. The static margin constraint was first satisfied at the 24th iteration that the takeoff mass was also increased considerably. After that the takeoff mass was relatively constant as the static margin was tied to its lower bound, i.e. G(6) = 0. Note that a realistic starting point of the design was generally preferred in order to avoid divergence and to reduce computational time during the optimization process. According to the results obtained from the design tool, the optimum configurations of AU3 and NU3 designs are modeled as illustrated in Figs. 4.5 and 4.6, respectively. The average computational time to obtain an optimum design was about 180 minutes on Intel Pentium 4, CPU 3.00 GHz and 1.00 GB of RAM.



a) Basic wing at design point.



b) Elevon deflection functioning as aileron at design point.



c) Elevon deflection functioning as elevator at takeoff.

Fig. 4.1 Lift coefficient distribution of the AU3 design.